UNIVERSITA' DEGLI STUDI DI MILANO

FACOLTA' DI MEDICINA VETERINARIA

SCUOLA DI DOTTORATO

Sanità e produzioni animali: Scienza, Tecnologia e Biotecnologie

Dipartimento di Scienze Veterinarie e Sanità Pubblica

Dottorato di Ricerca in Igiene Veterinaria e Patologia Animale

XXVI Ciclo

The role of pathology in the development and evaluation of murine xenograft models of human cancer

Docente guida: Prof. Eugenio Scanziani

Coordinatore del Dottorato: Prof. Giuseppe Sironi

Tesi di Dottorato di Ricerca
Dott. Vittoria CASTIGLIONI
Matricola n°R09078

ANNO ACCADEMICO 2012/2013

Contents **Pag**

Preface

Animal models are extensively used to understand how cancer develops and spreads throughout the body and to test the efficacy of new therapeutic drugs (Céspedes et al., 2006; Morton and Houghton, 2007; Workman et al., 2010). Preclinical cancer studies carried out on animal models fall into two broad categories:

- those using tumor cell transplantation;
- those in which tumors arise or are induced in the host.

Transplantation tumor models involve the transplantation of mouse or rat tumor cells into a host of the same species and strain (syngeneic or allograft) or the growth of human tumor cells into mice (xenograft) that are immunodeficient to prevent rejection. Syngeneic models have the advantage to use conventional rodents and normal housing conditions and mimic immune and stromal interactions, but are not applicable if investigating human-specific parameters. On the other hand, xenograft models do not allow the study of the interaction with the host immune system and have in general limited metastastic potential. The simplest approach to engraft transplantable tumors is subcutaneously (s.c.). This technique is easily performed and allows a daily monitoring of tumor growth, but it should be considered that the subcutis is an ectopic site for most tumors and metastases rarely develop from subcutaneously implanted tumors. Orthotopic transplantation of human tumor xenografts in immunosuppressed mice implies grafting a tissue in its natural location thus better reproducing the clinical behavior of the tumor (Céspedeset al., 2006; Richmond and Su, 2008), but on the other hand is a time consuming, expensive and technically challenging approach (Richmond and Su, 2008). Furthermore, an additional engrafting method relies on the implant of tumor cells within the peritoneal cavity (i.p.), thus maximizing the chance of transcoelomatic spread.

The successful engraftment of human tumors largely relies on the immunodeficient state of mice. Briefly, there are several degrees of immunocompromission in mice, listed below in a progressively severe grade of immunodeficiency:

- **nude mice** are athymic homozygotes for the nude spontaneous mutation (Foxn1$^{nu/nu}$) and lack T cells and are thus incapable of cell-mediated immunity, with a partially defective B cell development. Furthermore, they have an abnormal hair growth, so that subcutaneously transplanted tumors are easily visible and measurable;
- **Rag1 mice** are homozygotes for *Rag*1^{tm1Mom} knockout mutation and do not produce mature T or B cells, thus being more immunocompromised than nude ones. However, they do have an intact innate immunity;
- **non-obese diabetic or NOD mice** are homozygous for the severe combined immune deficiency spontaneous mutation (*Prkdc*^{scid} or *scid*) and have severely compromised innate and

adaptive immunity, lacking both B and T lymphocytes, reduced NK cell activity and impaired complement pathway (Kavirayani and Foreman, 2010);

- **NOD.Cg-Rag1^{tm1Mom}Prf1^{tm1Sdz}** are double homozygous knockout on the NOD background, with no mature T or B cells, no detectable NK cell cytotoxic activity and no serum immunoglobulin;
- **NOD.Cg-Prkdc^{scid} B2m^{tm1Unc}**are double homozygous knockout on the NOD background. These mice are MHC I-deficient, B and T cell-deficient, complement deficient and have few NK cells;
- **NOD.Cg-Prkdc^{scid}Il2rg^{tm1Wjl}**, also known as **NOD *scid* gamma (NSG)**, lack mature T, B, functional NK cells, hemolytic complement and are deficient in signaling in multiple cytokines, such as IL2, IL4, IL7, IL9, IL15 and IL21 (Foreman et al., 2011);
- **NOD.Cg-Rag1^{tm1Mom}Il2^{tm1Wjl}**, also known as **NOD-*Rag1 gamma* (NRG)**, are as severely immunocompromised as NSG, but tolerate much higher levels of irradiation.

The predictive value of these models has been extensively debated. The usefulness of these *in vivo* models of cancer will depend on how close they replicate the human disease. The major advantages of xenografts models are that they recapitulate growth, histopathological features and biological behavior of the original cancers, such as protein expression, tumor biomarker status and genomic and genetic status. On the other hand, they lack tumor original microenvironment, especially tumor-associated stroma, the host immune system is lost because of immunocompromission induced in mice and the full manifestation of metastatic potential is generally hampered (Jin et al., 2010).

Autochthonous tumor models include two broad categories: those spontaneously arising in outbred or inbred rodents or induced by chemical carcinogens, radiation, viruses or bacteria and/or those from genetically engineered mice (GEM), whose genetic profile is altered such that one or more genes thought to be involved in transformation or malignancy are mutated, deleted or overexpressed.

During the course of my PhD, I dealt with a wide array of different experimental studies based on xenografting of primary human tumor tissue in immunodeficient mice. The aim of this thesis is to provide a basic panel for a pathological approach to human xenografts, with detailed references to subcutaneous (s.c.) xenograft models and intraperitoneal (i.p.) xenograft models and to promising metastatic models. The goals of my three-year-research are to discuss how each model has been utilized to provide insights into human cancer therapy and to provide an assessment of the strengths and limitations of each model.

Chapter 1- Subcutaneous xenografts

Subcutaneous xenografts are generally implanted within the subcutis of the flank. Implantation of tumor material is performed using a trochar or surgical formation of a small subcutaneous pocket (Workman et al., 2010). Appropriate anaesthetics must be used and post-implantation analgesia is also strongly recommended. This technique implies advantages such a minimal technical effort to perform the engraftment and tumor growth can be monitored extremely easily through daily caliper measurements.

1.1 - Sampling

To maximize histopathological studies, subcutaneous xenografts should be collected with broad borders, involving skin and with fascial/subcutaneous tissues, as depicted in Figure 1.

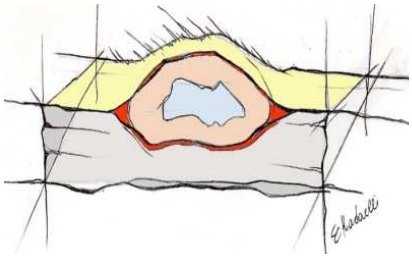

Fig. 1. Correct sampling technique of a subcutaneous xenograft.

This approach would allow a proper orientation of the sample, keeping topographic relations between human neoplastic cells and surrounding murine tissues, and would allow to evaluate xenograft-surrounding microenvironment cross-talk, with peculiar emphasis on capsular reaction, infiltrative *vs* expansile growth and peritumoral vessel embolization. Furthermore, adjacent normal tissues could be used as inner positive and/or negative controls for further immunohistochemical (IHC) trials.

Further details regarding sampling procedures are provided in Figures 2 to 4.

Fig. 2. To optimize the procedure, the xenograft can be placed on dry tissue paper after sampling and put in formalin.

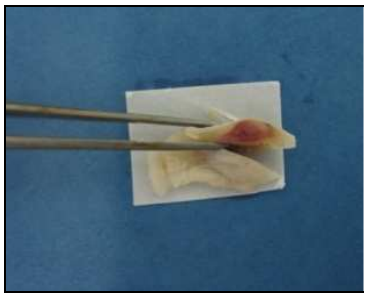

Fig. 3. After an optimal 48-hour-fixation period in 10% buffered formalin the sample can be trimmed.

Fig. 4. Trimmed samples are then put in a biocassette, ready for paraffin embedding.

1.2- General evaluation

For histopathological examination 4 µm sections from each tumor xenograft are routinely stained with Hematoxylin and Eosin (HE) and evaluated under a light microscope. Briefly, a general description of the tumor xenograft according to the Armed Forces Institute of Pathology (AFIP) guidelines is provided and specific parameters summarized in Table 1 are evaluated for each xenograft.

Tab. 1. Histopathological parameters evaluated for the analysis of subcutaneous xenografts.

Evaluated parameter	Description
Prevalent pattern of growth	Solid areas; lobules; tubules; acini; bundles; packets; etc.
Necrosis	0 = no intratumoral necrotic foci; 1 = necrotic foci accounting for less than 20% of tumor extension; 2 = necrotic foci comprised between 20% and 50% of tumor extension; 3 = necrotic foci comprised between 50% and 70% of tumor extension; 4 = necrotic foci accounting for more than 70% of tumor extension.
Stroma	0 = no stroma; 1 = scant amount of stroma mainly characterized by delicate fibrovascular septa separating groups of neoplastic cells; 2 = moderate amount of stroma characterized by a combination of delicate fibrovascular septa and broad bundles of fibrous connective tissue separating and embedding groups of neoplastic cells; 3 = abundant stroma mainly composed of broad bundles of fibrous connective tissue separating and embedding groups of neoplastic cells.
Peripheral invasion	0= absent 1= focal 2= multifocal 3= diffuse
Capsule	0= absent 1= present
Mitoses	Number of mitoses in 3 randomly selected high power fields (HPF=400x)
Apoptoses	Number of apoptotic cells in the same 3 high power fields evaluated for mitotic index (HPF=400x)

This evaluation is generally performed in a blind fashion and data are associated with different study groups only afterwards.

An example of this approach is reported below.

Experiment I - General approach to a subcutaneous xenograft

In collaboration with IRCCS, Istituto Nazionale dei Tumori of Milan the effects of several preclinical antitumor agents were tested on pediatric sarcoma xenografts.

The aim of this study was to evaluate the effects of compound exhibiting a pleiotropic activity on proliferative/survival pathways on tumor mitotic/apoptotic rate in a pediatric rhabdomyosarcoma cell line.

Material and Methods

Nude CD1 Swiss female mice were injected subcutaneously with human rhabdomyosarcoma cells (RD) and divided into 2 groups:

-control (CRL, mice 1, 5, 9, SS);

-mice treated with the tested compoud (Cpt 1, mice 1, 2, 5, 7).

Excised tumor xenografts and adjacent tissues were routinely formalin fixed and paraffin embedded. Four µm sections from each tumor xenograft were routinely stained with Hematoxylin-Eosin (HE) and evaluated under a light microscope for histopathological examination. A description of the general phenotype of tumors was made and histological evaluation of main morphological features previously outlined has been performed according to the criteria proposed in Table 1.

Results

In general, the following morphological features were observed in all examined samples: densely cellular, well demarcated, partially encapsulated nodular mass, expanding subcutis and occasionally the mammary fat pad. The mass was composed of solid areas, with scant to moderate fibrovascular stroma. Neoplastic cells were polygonal to spindled, ranging from 20 to 40 µm in diameter, with variably indistinct cell borders, an intermediate nuclear to cytoplasmic (N/C) ratio and a moderate amount of pale eosinophilic homogeneous cytoplasm. Nuclei were polygonal, 15 µm in diameter, central, with vesicular chromatin and occasional 1-2 central prominent magenta nucleoli. High mitotic activity, often with atypical mitotic figures, mild anisocytosis and anisokaryosis, large numbers of apoptotic cells and intratumoral necrotic and hemorrhagic foci, occasionally with dystrophic mineralization were present. Exemplificative pictures are provided in Figures 5 and 6.

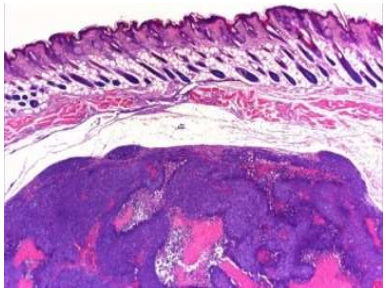

Fig.5. Subcutaneous undifferentiated, well demarcated solid xenograft with intratumoral broad areas of necrosis and hemorrhages. HE, 25x.

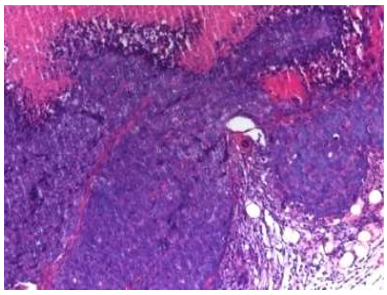

Fig.6. Close up of Fig.5. Note bundles of fibrous connective tissue separating solid areas of neoplastic cells. HE, 100x.

The histological evaluation of the main morphological features of examined xenografts is reported in Table 2 and summarized in Table 3.

Tab.2. Histopathological parameters from experiment I.

Sample	Prevalent pattern of growth	Necrosis	Stroma	Peripheral invasion	Mitoses			Apoptoses		
					in 3 HPF	Mean	Tot.	in 3 HPF	Mean	Tot.
1 CTR	solid	3	1	0	7; 4; 5	5,3	16	3; 2; 3	2,7	8
5 CTR	solid	3	2	0	8; 16; 7	10,3	31	1; 1; 4	2	6
9 CTR	solid	3	1	0	7; 4; 7	6	18	1; 6; 2	3	9
SS CTR	solid	3	1	0	11; 15; 6	10,7	32	3; 2; 1	2	6
Mean		**3**	**1,2**	**0**		**8,1**	**24,2**		**2,4**	**7,2**
1 Cpt1	solid	3	1	0	2; 3; 9	4,7	14	9; 4; 2	5	15
2 Cpt1	solid	2	1	0	6; 5; 5	5,3	16	1; 2; 2	1,7	5
5 Cpt1	solid	4	2	0	0; 0; 0	0	0	4; 8; 10	7,3	22
7 Cpt1	solid	1	1	0	8; 7; 4	6,3	19	7; 6; 2	5	15
Mean		**2,5**	**1,2**	**0**		**4,1**	**12,2**		**4,7**	**14,2**

Tab.3. Summary of the mean scores of histological results and of the mean numbers of mitoses and apoptosis reported in Tab.2.

Group	Necrosis	Stroma	Mitoses		Apoptoses	
			Mean	Tot	Mean	Tot
CTR	3	1,2	8,1	24,2	2,4	7,2
Cpt1	2,5	1,2	4,1	12,2	4,7	14,2

Comments

Overall, tumor xenografts from experiment I had a similar pattern of growth (solid) and a similar behavior, with no peripheral invasion observed. Tumors were well demarcated, nodular and partially encapsulated.

A trend towards decreased intratumoral necrosis and decreased mitotic index, with increased apoptotic index was observed in treated group compared to control one.

In conclusion, an interference on tumoral proliferative/survival pathways elicited by the tested compound was confirmed by this pivotal study.

1.3- Evaluation of specific parameters and treatment-associated changes

During the 3-year-period of my PhD, I evaluated changes in tumor growth and morphology associated with different therapeutic treatments. Parameters modulated by pharmacological trials mainly addressed tumor vasculature (angiogenesis) and the number and type of intratumoral mitoses and apoptosis.

1.3.1 Evaluation of angiogenesis

Angiogenesis or neovascularization refers to blood vessel formation in adults. It arises both is physiologic scenarios, such as wound healing and in pathologic processes, such as solid tumor development and metastasis (Folkman, 2003; Folkman, 2007), so that angiogenesis is one of the "hallmarks of cancer" designed by Hanahan and Weinberg in 2011. In light of these considerations, drugs targeting tumor vasculature can be regarded as a potential strategy in the therapy of tumors. Antiangiogenic agents have provided only modest benefit as monotherapy, whereas their use in combination with conventional cytotoxic chemotherapies has lead to maximal benefit because such combinations would destroy two separate compartments of tumors, cancer cells and endothelial cells (Gasparini et al., 2005; Volk et al., 2008). On the other hand, tumor vasculature may influence the delivery and effectiveness of anticancer therapy (Yu et al., 2002).

The major goal of an antiangiogenic therapy is the reduction of the **number** of vessels. The measurement of angiogenesis is inherently difficult since it is a dynamic process. The vast majority of studies have focused so far on the product of angiogenesis, the **microvessel density** (**MVD**) (Hasan et al., 2000). The assessment of MVD in "vascular hot spots" with the aid of immunohistochemistry (IHC) for endothelial cells is the conventional method for evaluating angiogenesis in human oncology, but also other morphometric parameters, such as the immunolabelled endothelial area (**EA**) can be evaluated with the aid of digital image analysis (DIA).

Another feature is **vascular morphology**. Tumor vasculature is generally structurally and functionally abnormal (Jain, 2005), characterized by leaky, tortuous, dilated and saccular vessels, with decreased pericyte coverage and abnormal basement membrane, due to an imbalance between proangiogenic and antiangiogenic factors (McDonald and Choyke, 2003; Thorpe, 2004; Baluk et al., 2005). As a consequence, tumor blood flow is impaired, thus resulting in high interstitial fluid pressure, hypoxic regions within the tumor, acidosis and impaired drug delivery (Jain,2005; Hagendoorn et al., 2007).

An additional parameter that could be assessed after vessel number and morphology is **vascular maturity**, in which pericytes are involved. Pericytes are long, slender, plastic cells of mesenchymal origin that have long been regarded as supporting cells. Pericytes do express protein typical of

contractile cells, such as smooth muscle-specific isoforms of actin and myosin (Díaz-Flores et al., 1991) and are closely apposed to the outer surfaces of the endothelial tubes in normal tissue vasculature, thus providing mechanical and physiologic support (Hirschi and D'Amore, 1996; Gerhardt and Betsholtz, 2003). Tumor-associated vasculature, in contrast, generally lacks appreciable coverage by these auxiliary cells.

Traditionally, intra-tumoral microvessels can be identified by immunostaining of endothelial cells with specific antibodies, such as CD31, a pan-endothelial marker that can be used on paraffin sections. CD31, also known as "platelet endothelial cell adhesion molecule-1" (PECAM-1), can be found on the surface of endothelial cells and to a slightly lesser extent on platelets and leukocytes. Another usefully applied antibody is Factor VIII-related antigen (FVIIIra), also known as von Willebrand factor (vWF), synthesized by endothelial cells and megakaryocytes and mediating platelet adhesion to the walls of injured vessels. Immunohistochemical detection of CD31 and FVIIIra-positive vessels has been extensively used to quantify angiogenesis of xenograft tumors in immunodeficient animal models carrying various human tumor cell loads (Vanzulli et al., 1997; Fulzele et al., 2006; Muruganandham et al., 2006; Ragel et al., 2007), although the superiority of CD31 over FVIIIra as a marker for angiogenesis in various xenograft models has recently been established (Wang et al., 2008).

Beside blood vessels, also lymphatics can be highlighted by immunohistochemistry and several specific markers have been identified. These include VEGFR-3, the tyrosine kinase receptor for vascular endothelial growth factor (VEGF)-C and VEGF-D (Kaipainen et al., 1995; Joukov et al., 1996; Achen et al., 1998); podoplanin, a glomerular podocyte membrane mucoprotein (Breiteneder-Geleff et al., 1999); Prox-1, the homebox gene product that is involved in developmental regulation of the lymphatic system (Wingle and Oliver, 1999); a hyaluronan cell surface receptor on lymphatic endothelial cells, LYVE-1 (Jackson et al., 2001) and desmoplakin (Ebata et al., 2001).

The evaluation of angiogenesis is part of published paper by Rovida et al.(2013) listed in Appendix 1 and examples of studies centered on angiogenesis evaluation I performed over my 3-year-PhD period are reported below.

Experiment II -Evaluation of MVD in pediatric sarcoma xenografts

In collaboration with IRCCS, Istituto Nazionale dei Tumori of Milan the effects of several preclinical angiogenesis inhibitors were tested on pediatric sarcomas xenografts.

The aim of this study was to evaluate the effects of inhibitors of pathways mediated by angiogenic factors, including bFGF and VEGF family members, on tumor MVD in pediatric rhabdomyosarcoma cell lines (Exp. A and Exp. B) and in Ewing's sarcoma cell line SK-N-MC (Exp. C).

Material and Methods

Exp. A -Nude CD1 Swiss female mice were injected subcutaneously with human rhabdomyosarcoma cells (RD) and divided into different groups of treatment:
-control mice (CRL, mice 1, 5, 9, SS);
-mice treated with test inhibitor (Inhib1, mice 1, 2, 5, 7).

Exp. B -Nude CD1 Swiss female mice were injected subcutaneously with human rhabdomyosarcoma cells (RD) and divided into different groups of treatment:
-control mice (CRL, mice 1, 2, 3, 4, 5, 6, 7, 8);
-mice treated with test inhibitor (Inhib 1, mice 9, 10, 11, 14, 15, 16);
-mice treated with Sorafenib (SORAFENIB, mice 18, 19, 20, 21, 22, 24).

Exp. C - Nude CD1 Swiss female mice were injected subcutaneously with human Ewing's sarcoma cells (SK-N-MC) and divided into different groups of treatment:
-control mice (CRL, mice 2, 3, 4, 6, 7);
-mice treated with test inhibitor, early treatment (Inhib1 early, mice 3, 5, SS);
-mice treated with test inhibitor, late treatment (Inhib1 late, mice 1, 2, 4).

Overall, excised tumor xenografts and adjacent tissues were routinely formalin fixed and paraffin embedded. To assess the extent of tumor angiogenesis, 4 µm sections from each tumor xenograft were immunostained with a primary rat monoclonal antibody against CD31 (PECAM) antigen (Dianova; clone SZ31). For each sample, serial sections incubated with a 10% solution of normal goat serum served as negative controls. For further information a detailed list of all primary antibodies and immunohistochemical procedures tested are reported in Table n° 15 at the end of Chapter 1. The number of CD31-positive vascular outlines were counted using the ImageJ analysis program (http://rsb.info.nih.gov/ij/) in three 200x microscopic fields randomly selected throughout the neoplastic tissue, avoiding necrotic areas and the capsule.

Results

Results regarding MVD from the 3 experiments are reported in Tables 4 to 6.

Tab. 4. Results regarding MVD in Exp. A.

Exp	Sample	Field #1	Field #2	Field #3	tot	mean
A	**1 CTR**	4	3	2	9	3
	5 CTR	2	7	3	12	4
	9 CTR	15	9	6	30	10
	SS CTR	6	22	19	47	15,7
	Mean				**24,5**	**8,2**
	1 Inhib1	4	4	5	13	4,3
	2 Inhib1	5	6	14	25	8,3
	5 Inhib1	0	0	0	0	0
	7 Inhib1	6	8	10	24	8
	Mean				**15,5**	**5,2**

Tab. 5. Results regarding MVD in Exp. B.

Exp	Sample	Field #1	Field #2	Field #3	tot	mean
B	**1 CTR**	9	5	6	20	6,7
	2 CTR	9	6	6	21	7
	3 CTR	6	4	7	17	5,7
	4 CTR	15	10	13	38	12,7
	5 CTR	21	12	10	43	14,3
	6 CTR	11	9	9	29	9,7
	7 CTR	17	9	5	31	10,3
	8 CTR	9	7	18	34	11,3
	Mean				**29,1**	**9,7**
	9 Inhib1	17	4	10	31	10,3
	10 Inhib1	6	13	5	24	8
	11 Inhib1	3	6	6	15	5
	14 Inhib1	8	4	10	22	7,3
	15 Inhib1	5	4	7	16	5,3
	16 Inhib1	2	11	7	20	6,7
	Mean				**21,3**	**7,1**
	18 Sorafenib	9	7	6	22	7,3
	19 Sorafenib	4	2	3	9	3
	20 Sorafenib	4	6	6	16	5,3
	21 Sorafenib	6	6	3	15	5
	22 Sorafenib	1	5	3	9	3
	24 Sorafenib	8	6	1	15	5
	Mean				**14,3**	**4,8**

Tab. 6. Results regarding MVD in Exp. C.

Exp	Sample	Field #1	Field #2	Field #3	tot	mean
C	**2 CTR**					
	3 CTR	14	15	8	37	12,3
	4 CTR	9	20	17	46	15,3
	6 CTR	10	6	13	29	9,7
	7 CTR	5	11	10	26	8,7
	Mean				**34,5**	**11,5**
	3 Inhib1 early					
	5 Inhib1 early	5	14	4	23	7,7
	SS Inhib1 early	2	6	1	9	3
	Mean				**16**	**5,3**
	1 Inhib1 late	4	4	8	16	5,3
	2 Inhib1 late					
	4 Inhib1 late	6	16	12	34	11,3
	Mean				**25**	**8,3**

Exemplificative pictures of immunohistochemical staining are provided in Figures 7 and 8.

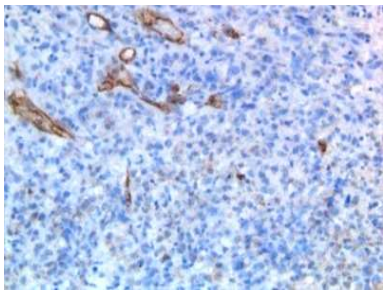

Fig. 7. Randomly selected 200x field from a CRL animal from Exp. A. Note the large numbers of CD31-positive vessels.

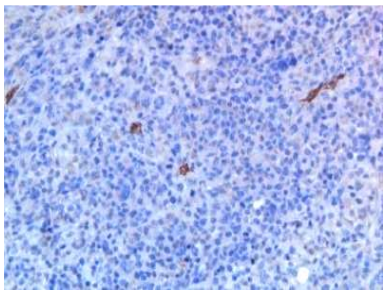

Fig. 8. Randomly selected 200x field from an animal from Exp. A treated with HPA-inib. Note the reduced number of CD31-positive vessels compared to CRL mouse.

Comments

Overall, a decrease in the number of vessels in treated groups was noticed compared to control ones.

In experiment C, Sorefenib was additionally tested. Sorafenib is a known inhibitor of angiogenesis, through inhibition of several receptor tyrosine kinases, such as VEGFR and PDGFR, which mediate the signaling of pro-angiogenic factors.

In conclusion, the expected role of the tested angiogenesis inhibitor and Sorafenib in decreasing microvessel density in examined pediatric sarcoma xenograft models was confirmed by this pivotal study.

Experiment III- Evaluation of vascular maturity in an allograft model of 3LL

In collaboration with Istituto Mario Negri of Milan the effects of Sunitinib on MVD and vascular maturity were assessed on murine pulmonary carcinoma Lewis Lung (3LL) implanted intramuscularly in mice. Please note this model is not a human xenograft, but an allograft model. The pathological approach to the evaluation of the samples would be identical if applied to a xenograft model.

The aims of this study were to evaluate MVD and vessel maturation of 3LL implanted in the tibial muscle of mice.

Material and Methods

C57/BL6 mice were injected within the tibial muscle with 3LL cell line. The experiment was performed twice and mice were divided into control group and animals treated with Sunitinib. To assess vascular maturity, pericyte coverage of blood vessels was investigated through double immunofluorescence staining with CD31 and SMA and digital image analysis. 4 µm sections from each tumor allograft were immunostained with a primary rat monoclonal antibody against CD31 (PECAM) antigen (Dianova; clone SZ31) and with a primary rabbit polyclonal antibody against Smooth muscle actin (LabVision; RB-9010). Sections were then incubated with Alexa fluor anti-rat and Alexa fluor anti-rabbit dyes. For each sample, serial sections incubated with a 10% solution of normal goat serum served as negative controls. The number of CD31-positive vascular outlines (green fluorescence) and the number of CD31 and SMA-positive vascular outlines (green and red fluorescence) were counted using the ImageJ analysis program (http://rsb.info.nih.gov/ij/) in five 200x microscopic fields randomly selected throughout the neoplastic tissue.

Results

Results are summarized in Table 7.

Tab. 7. Numbers of CD31 and CD31 and SMA-positive vessels within 3LL allograft model.

Exp	Group	Sample	Field #1 CD31	Field #1 CD31 and SMA	Field #2 CD31	Field #2 CD31 and SMA	Field #3 CD31	Field #3 CD31 and SMA	Field #4 CD31	Field #4 CD31 and SMA	Field #5 CD31	Field #5 CD31 and SMA	tot CD31	mean CD31	tot CD31 and SMA	mean CD31 and SMA
1	SUNITINIB	#326	11	0	7	0	6	0	15	0	29	0	68	13,6	0	0
		#327	14	0	14	0	7	0	20	0	17	0	72	14,4	0	0
		#403	13	0	14	0	16	0	16	1	11	3	70	14	4	0,8
		#417	15	0	11	0	12	0	15	0	16	0	69	13,8	0	0
		#422	18	0	16	0	10	0	9	0	15	0	68	13,6	0	0
		mean											**69,4**	**13,9**	**0,8**	**0,2**
	CRL	#338	43	0	28	0	33	0	34	0	24	0	162	32,4	0	0
		#404	23	0	33	0	15	0	19	1	17	0	107	21,4	1	0,2
		#408	24	0	35	0	22	0	8	0	14	0	103	20,6	0	0
		#423	45	0	25	0	23	0	48	0	48	0	189	37,8	0	0
		#432	45	0	51	0	41	1	56	0	46	0	239	47,8	1	0,2
		mean											**160**	**32**	**0,4**	**0,1**
2	SUNITINIB	#342	15	0	13	1	8	0	12	1	14	0	62	12,4	2	0,4
		#352	20	0	14	0	19	0	5	0	15	0	73	14,6	0	0
		#361	10	0	8	0	7	0	8	1	5	0	38	7,6	1	0,2
		mean											**57,7**	**11,5**	**1**	**0,2**
	CRL	#306	46	0	56	0	28	0	49	0	52	0	231	46,2	0	0
		#847	31	0	38	0	33	0	47	0	38	0	187	37,4	0	0
		#859	34	0	38	0	30	0	29	0	60	0	191	38,2	0	0
		mean											**203**	**40,6**	**0**	**0**

Exemplificative pictures are provided in Figures 9 to 11.

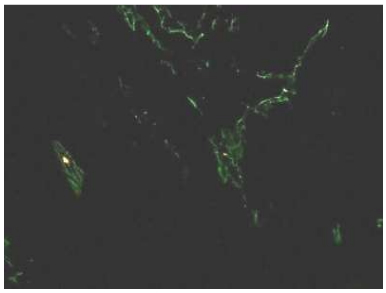

Fig. 9. 200x randomly selected field with CD31-positive endothelial cells.

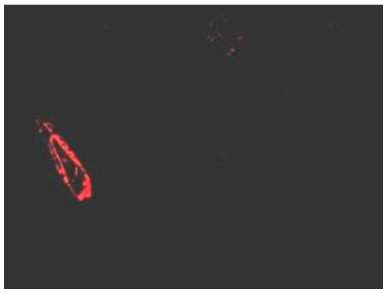

Fig. 10. Same field of Fig. 9 with a SMA-positive vascular outline.

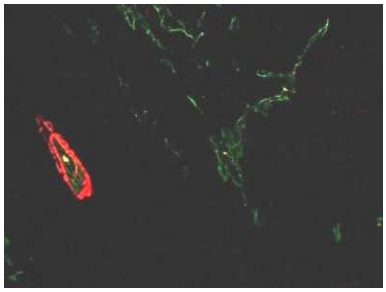

Fig. 11. This picture is obtained by merging of the two previous Figures.

Comments

Results obtained from 2 different experiments after Sunitinib-treatment recapitulate those reported by current literature, with Sunitinib resulting in a reduction of MVD and in an increased pericyte vascular coverage, in the context of vascular normalization after treatment of tumors with angiogenesis inhibitors (Goel et al., 2011; Griffioen et al., 2012).

In conclusion, not only a reduction in MVD, but also the so-called “normalization” of residual vessels were confirmed by these two experiments after pharmacological treatment. Jain (2005) hypothesized that antiangiogenic agents can transiently “normalize” the abnormal structure and function of tumor vasculature, thus making the delivery of oxygen and chemotherapeutic drugs more efficient. Changes in tumor microenvironment, with a decreased microvessel density and vessel area, and in vessel morphology, with less leaky, less dilated, less tortuous vessels with a normal basement membrane and increased pericyte coverage, decreased interstitial fluid pressure and hypoxia after antiangiogenic/VEGF therapy have been demonstrated by several investigators (Wildiers et al., 2003; Winkler et al, 2004; Tong et al., 2004; Dickson et al, 2007) and were confirmed by the aforereported results.

1.3.2 Evaluation of aberrant mitoses

The evaluation of aberrant mitoses is part of published papers by Colombo et al.(2012) and by Pilkington-Miksa et al.(2012) listed in Appendix 1 and an example of a study centered on this type of evaluation is reported below.

Experiment IV-Evaluation of aberrant mitoses

In collaboration with IRCCS, Istituto Nazionale dei Tumori of Milan the effects of Paclitaxel in comparison with two novel drugs (Ligand 1 and of Compoud 21) were tested on subcutaneous xenografts of human ovarian carcinoma.

Briefly, Paclitaxel (PTX) is an anti-neoplastic drug known to arrest cells in mitosis. No information regarding Ligand 1 and Compoud 21 were provided.

The aim of this study was to evaluate the effect of Paclitaxel, Ligand 1 and Compound 21 on mitotic index and mitotic morphology in subcutaneous xenografts of human ovarian carcinoma.

Material and Methods

Cisplatin-resistant human ovarian carcinoma cell lines (IGROV-1/Pt1) were subcutaneously injected in nude athymic (nu/nu) female mice. Mice were divided in the following groups of treatment:

-control mice (CRL, mice 1, 2, 3, 4);

-mice treated with Ligand 1 (mice 5, 6, 7, 8);

-mice treated with Compound 21 (mice 9, 10, 11, 12);

-mice treated with Paclitaxel (PTX, mice 13, 14, 15, 16).

Four µm sections from each tumor xenograft were routinely stained with Hematoxylin-Eosin (HE) and evaluated under a light microscope. Mitoses were evaluated in three randomly selected 400x fields within the bulk of the xenografts, avoiding areas of necrosis and hemorrhage. The total number of mitoses and the mean value for each sample were evaluated. Furthermore, mitoses were distincted in “normal” and “aberrant”, considering in this latter class both small condensed hyperchromatin nuclei and large cells composed of a nuclear envelope around individual clusters of misaggregated chromosomes (mitotic catastrophe), according to Portugal et al.(2010). The ratio between the number of aberrant mitoses and total number of mitoses was evaluated. The evaluation of mitoses was performed in a blind fashion and only afterwards data were associated with corresponding mice.

Results

The number of mitoses further classified as “normal” (N) and “aberrant” (A) observed in the different groups of treatment is reported in Table 8.

Tab. 8. The number of normal, aberrant and total mitoses is reported for each examined animal.

Group	Sample	#1			#2			#3			mean	tot
		N	A	TOT	N	A	TOT	N	A	TOT		
CRL	#1	3	0	3	8	0	8	1	0	1	4	12
	#2	6	0	6	6	0	6	2	0	2	4,7	14
	#3	4	0	4	11	2	13	3	1	4	7	21
	#4	4	1	5	6	0	6	5	0	5	5,3	16
Mean											**5,2**	**15,7**
Ligand1	#5	8	1	9	6	0	6	2	1	2	5,7	17
	#6	3	0	3	8	1	9	6	0	6	6	18
	#7	3	1	4	3	0	3	4	0	4	3,7	11
	#8	0	3	3	6	0	6	9	0	9	6	18
Mean											**5,3**	**16**
Compound21	#9	5	22	27	4	2	6	0	62	62	31,7	95
	#10	0	43	43	0	30	30	0	17	17	30	90
	#11	2	3	5	9	2	11	7	7	14	10	30
	#12	6	9	15	9	3	12	2	3	5	10,7	32
Mean											**20,6**	**61,7**
PTX	#13	5	5	10	4	8	12	9	4	13	11,7	35
	#14	3	2	5	5	9	14	3	6	9	9,3	28
	#15	8	0	8	0	7	7	0	2	2	5,7	17
	#16	0	13	13	1	3	4	0	2	2	6,3	19
Mean											**8,2**	**24,7**

The ratio between aberrant and total number of mitoses is reported in Table 9 and summarized in Figure 12. An exemplificative picture of an aberrant mitosis is shown in Figure 13.

Tab.9. Ratio between normal vs aberrant mitoses.

Group	Sample	ratio field #1	ratio field #2	ratio field #3	mean
CRL	#1	0	0	0	0
	#2	0	0	0	0
	#3	0	0,15	0,25	0,13
	#4	0,2	0	0	0,1
	mean				**0,1**
Ligand1	#5	0,1	0	0,5	0,2
	#6	0	0,1	0	0,03
	#7	0,25	0	0	0,08
	#8	1	0	0	0,3
	mean				**0,2**
Compound21	#9	0,8	0,3	1	0,7
	#10	1	1	1	1
	#11	0,6	0,2	0,5	0,4
	#12	0,6	0,25	0,6	0,5
	mean				**0,7**
PTX	#13	0,5	0,7	0,3	0,5
	#14	0,4	0,6	0,7	0,6
	#15	0	1	0	0,3
	#16	1	0,75	1	0,9
	mean				**0,6**

Fig. 12. Ratio between normal *vs* aberrant mitoses in different groups of treatment.

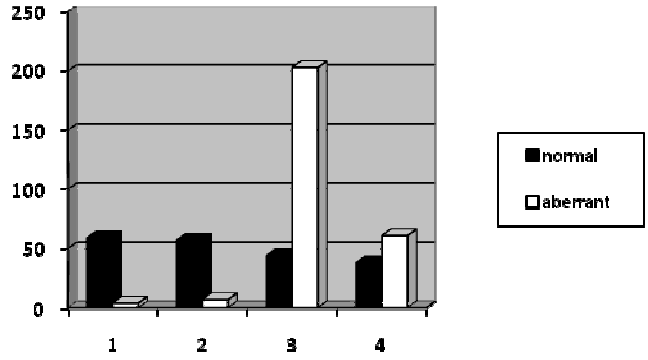

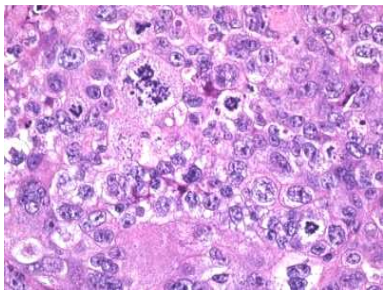

Fig. 13. Example of an aberrant mitosis from a mouse treated with Paclitaxel, HE.

Comments

Histological analysis highlighted an exceedingly higher number of mitoses in the group treated with Compound 21, compared to other ones. Furthermore, the majority of the mitoses observed in this group and in the group treated with PTX were aberrant.

The finding that the majority of mitoses observed in PTX-treated group were aberrant is consistent with the mechanism of action of the drug (Roninson et al., 2001; Portugal et al., 2010; Matson and Stukenberg, 2011). Paclitaxel is a spindle poison that arrests cells in mitosis, binding to tubulin within existing microtubules and stabilizing the polymer. When incubated with spindle poisons, the number of mitosis dramatically increases, with cells entering mitosis, but failing to exit and assuming an aberrant morphology, the so called “mitotic catastrophe” (Portugal et al., 2010), which is characterized by a nuclear envelope around individual clusters of misaggregated chromosomes.

In conclusion, the expected role of Paclitaxel was confirmed by this small pivotal study.

1.3.3 *Evaluation of apoptoses*

Apoptosis is a pathway of cell death that is induced by a tightly regulated program in which cells destined to die activate enzymes that degrade the cells' own nuclear DNA and nuclear and cytoplasmic proteins.

The evaluation of apoptoses is part of published paper by Lopergolo et al. (2013) listed in Appendix 1 and an example of a study centered on this type of evaluation is reported below.

Experiment V- Evaluation of apoptoses in medullary thyroid carcinoma xenograft

In collaboration with IRCCS, Istituto Nazionale dei Tumori of Milan the number of apoptosis was evaluated in human medullary thyroid carcinoma xenografts.

The aim of this study was to evaluate the effect of Cisplatin and Sunitinib on the number of apoptoses observed in human medullary thyroid carcinoma xenografts.

Material and methods

Human medullary thyroid carcinoma cells (MZ CRC-1 cells) were injected subcutaneously in SCID mice and sacrificed at day 38. Mice were divided into different groups of treatment:

-control mice (CRL, mice 1, 2, 3);

-mice treated with Cisplatin (mice 4, 5, 6);

-mice treated with Sunitinib (mice 7, 8, 9);

-mice treated with a combination of Cisplatin and Sunitinib (mice 10, 11, 12).

Four µm sections from each tumor xenograft were routinely stained with Hematoxylin-Eosin (HE) and evaluated under a light microscope. Furthermore, to quantify the number of apoptoses, 4 µm sections from each tumor xenograft were immunostained with a primary rabbit polyclonal antibody against the active form of caspase (Cell Signalling, clone Asp175). For each sample, serial sections incubated with a 10% solution of normal goat serum served as negative controls. The ratio between the total number of caspase positive-neoplastic cells and the total number of neoplastic cells (apoptotic index) was calculated using the ImageJ analysis program (http://rsb.info.nih.gov/ij/) in six 400x microscopic fields randomly selected within the bulk of the xenograft, avoiding necrotic areas and the capsule. Focally clustered labeled nuclear "dust" (free apoptotic bodies) were counted as 1 cell.

Results

Analysis of HE stained sections, with peculiar emphasis on the evaluation of apoptoses is reported in Table 10.

Tab. 10. Histopathological parameters from Experiment V.

Group	Sample	Prevalent pattern of growth	Necrosis	Stroma	Peripheral invasion	Capsule	Mitoses			Apoptoses		
							in 3 HPF	Mean	Tot	in 3 HPF	Mean	Tot
Crl	#1	lobules	1	2	0	1	10;11;7	9,3	28	0;3;0	1	3
	#2	solid	1	1	0	1	3;7;6	5,3	16	3;2;1	2	6
	#3	solid	1	2	0	1	10;4;5	6,3	19	1,7;2	3,3	10
Mean			**1**	**1,7**	**0**	**1**		**7**	**21**		**2,1**	**6,3**
Cisplatin	#4	solid areas	1	2	0	1	3;3;2	2,7	8	27;9;17	17,7	53
	#5	lobules	1	2	0	1	1;5;0	2	6	16;24;18	19,3	58
	#6	solid areas	1	2	0	1	1;0;1	0,7	2	30;27;15	24	72
Mean			**1**	**2**	**0**	**1**		**1,8**	**5,3**		**20,3**	**61**
Sunitinib	#7	solid areas	3	2	0	1	0;2;4	2	6	7;10;13	10	30
	#8	solid	1	1	0	1	3,3;1	2,3	7	6;11;1	6	18
	#9	lobules	1	2	0	1	1;1;4	2	6	6;8;7	7	21
Mean			**1,7**	**1,7**	**0**	**1**		**2,1**	**6,3**		**7,7**	**23**
Cisplatin + Sunitinib	#10	solid	1	2	0	1	0;0;2	0,7	2	39;67;23	43	129
	#11	solid	2	2	0	1	2;0;0	0,7	2	40:17;50	35,7	107
	#12	solid	1	3	0	1	0;0;1	0,3	1	94;90;55	80	239
Mean			**1,3**	**2,3**	**0**	**1**		**0,6**	**1,7**		**52,9**	**158,3**

Aforereported results are summarized in Table 11.

Tab. 11. Mean histopathological scores and mean numbers of mitoses and apoptoses shown in Tab.10.

Group	necrosis	stroma	mitoses		apoptoses	
			mean	tot	mean	tot
Crl	1	1,7	7	21	2,1	6,3
Cisplatin	1	2	1,8	5,3	20,3	61
Sunitinib	1,7	1,7	2,1	6,3	7,7	23
Cisplatin + Sunitinib	1,3	2,3	0,6	1,7	52,9	158,3

Results obtained by Cleaved caspase-3 immunohistochemistry are reported in Table 12 and exemplificative pictures are provided in Figures 14 and 15.

Tab. 12. Immunohistochemical evaluation of apoptoses.

Group	Sample	Field	#1	#2	#3	#4	#5	#6	tot	apoptotic index
CRL	#1	pos nuclei	1	5	10	2	5	7	30	0,01
		tot nuclei	327	340	424	329	371	431	2222	
	#2	pos nuclei	3	0	2	8	0	4	17	0,01
		tot nuclei	365	380	430	368	316	329	2188	
	#3	pos nuclei	2	2	3	1	5	5	18	0,01
		tot nuclei	397	362	377	368	360	337	2201	
	Mean									0,01
CISPLATIN	#4	pos nuclei	19	16	9	37	10	17	108	0,05
		tot nuclei	382	341	368	317	244	315	1967	
	#5	pos nuclei	29	16	53	13	5	10	126	0,07
		tot nuclei	423	285	392	182	198	242	1722	
	#6	pos nuclei	48	20	14	22	16	15	135	0,06
		tot nuclei	400	319	378	371	294	290	2052	
	Mean									0,06
SUNITINIB	#7	pos nuclei	5	8	16	22	3	21	75	0,04
		tot nuclei	297	333	330	310	258	352	1880	
	#8	pos nuclei	6	16	4	6	4	3	39	0,02
		tot nuclei	353	384	240	268	239	319	1803	
	#9	pos nuclei	9	5	1	15	6	8	44	0,02
		tot nuclei	261	321	320	325	280	229	1736	
	Mean									0,03
CISPLATIN + SUNITINIB	#10	pos nuclei	39	28	22	26	10	44	169	0,09
		tot nuclei	375	317	311	331	151	336	1821	
	#11	pos nuclei	29	24	27	32	43	42	197	0,12
		tot nuclei	264	305	274	223	277	302	1645	
	#12	pos nuclei	50	57	65	28	45	48	293	0,16
		tot nuclei	293	398	337	236	267	262	1793	
	Mean									0,12

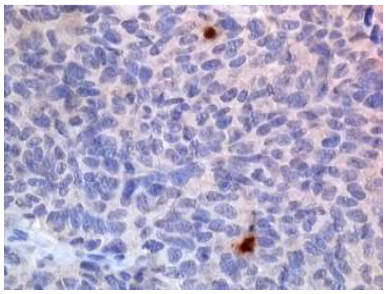

Fig. 14. Randomly selected high power field from sample #3 (control). Note the exceedingly low number of caspase-positive nuclei, stained in brown against the blue-counterstained ones. Cleaved-caspase 3 immunohistochemistry, 400x.

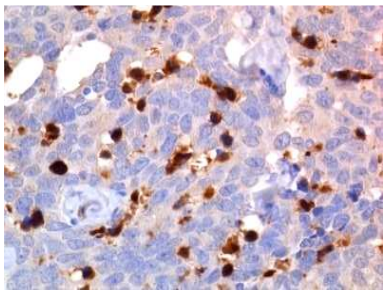

Fig. 15. Randomly selected high power field from sample #12 (Cisplatin+Sunitinib). Note the high number of caspase-positive nuclei, stained in brown against the blue-counterstained ones. Cleaved-caspase 3 immunohistochemistry, 400x.

Comments

Results obtained by immunohistochemistry recapitulated those obtained by evaluation of hematoxylin and eosin-stained sections. The highest number of apoptoses was observed in mice treated with both Cisplatin and Sunitinib.

Sunitinib is supposed to inhibit Ret, a proto-oncogene that is known to be mutated in medullary thyroid carcinomas (Nicolini et al., 2011), whereas Cisplatin elicits apoptosis both via the intrinsic (mitochondrial) pathway, causing DNA crosslinking and the extrinsic one, via CD95 (Fas) pathway. In conclusion, the exceedingly higher number of apoptosis observed in the group treated with the two combined drugs support the hypothesis of a synergic action between them.

1.4 -Matrigel plug assay

Briefly, the matrigel plug assay is based on the subcutaneous injection of an extract of basement membrane proteins (Matrigel) containing cells or substances to be tested. Matrigel is a soluble and sterile compound derived from the Engelbreth-Holm-Swarm (EHS) mouse sarcoma, a tumor rich in ECM proteins. Its major component is laminin, followed by collagen IV, heparan sulfate proteoglycan and entactin. After subcutaneous injection, Matrigel solidifies to form a plug that can be recovered after approximately 7-21 days in the animal and examined histologically (Passaniti et al., 1992). Matrigel supports cell morphogenesis, differentiation and tumor growth and furthermore growth factors and compounds can be added, thus enhancing cell growth, differentiation and/or angiogenesis.

An example of a study with Matrigel is reported below.

Experiment VI - Evaluation of an anti-tumor drug in a Matrigel plug assay

In collaboration with Istituto Mario Negri of Bergamo (BG) an experiment was designed to investigate the role of an anti-tumor drug of marine origin.

Tested compound is an antitumoral agent of marine origin that is reported to block the cell cycle and interfere with inducible gene transcription and to induce cytotoxic effects on monocytes and macrophages. According to current literature, a reduction in the number of tumor vessels and of F4/80-positive macrophages have been described after its administration (Germano et al., 2010).

The aim of this study was to evaluate vascular and lymphatic vessels and macrophagic infiltrate after administration of tested compound in mice injected with Matrigel alone or Matrigel added with bFGF.

Please note that no neoplastic cells either of human or murine origin were implanted within the Matrigel in this experiment, thus this study is different from the other ones presented.

Material and Methods

Mice were divided in different groups of treatment as follows:

-mice injected with empty matrigel (mice Crl - 1, 2, 3, 4, 5, 6, 7);

-mice injected with matrigel added with bFGF (mice Crl + 1, 2, 3, 4, 5, 6, 7);

-mice injected with matrigel and treated with tested compound, administered twice a day for 3 days (q2X3) at the dose of 0.1 mg/kg (mice 376, 377, 380, 381, 389, 393);

-mice injected with matrigel and treated with tested compound, administered once a day for 5 days (q1X5) at the dose of 0.1 mg/kg (mice 353, 356, 357, 358, 362, 363, 366).

Mice were sacrificed and the whole pellet encompassing skin and deep muscles was collected and fixed in 10% buffered formalin. Pellets were processed and embedded in paraffin, oriented along a transverse cut section and cut into serial sections of four-µm thickness and used for immunohistochemical analysis. CD31, LYVE-1 and F4/80 were the immunohistochemical markers used in this study to detect blood vessels, lymphatics and macrophagic infiltrate respectively. To establish microvessel density, area and morphology, formalin-fixed sections from each pellet were immunostained with the rat monoclonal anti-mouse CD31 antibody, a specific marker for endothelial cells (Dianova). The reaction was revealed by incubating the sections with 3,3'-diaminobenzidine (Vector Laboratories, Burlingame, CA). Hematoxylin counterstaining was done. Vascular hotspots (three fields in each sample when possible) were selected at 200X within the matrigel. These areas generally corresponded to the periphery of the pellet.

To estabilish lymphatic vessel density, area and morphology, formalin-fixed, paraffin-embedded sections from each group were immunostained with the rabbit polyclonal Lyve-1 antibody, a specific marker for lymphatic vessels (AbCam, clone 14917). The reaction was revealed by incubating the sections with 3,3'-diaminobenzidine (Vector Laboratories, Burlingame, CA). Hematoxylin counterstaining was performed.

Hotspots (three fields in each sample when possible) were selected at 200X within the matrigel. These areas generally corresponded to the periphery of the pellet.

Morphometric analysis for both vascular and lymphatic vessels were performed with Image-Pro Plus software.

The parameters collected were:

- vessel number (object count);
- vessel area (expressed in μm^2);
- mean vessel diameter (expressed in µm, is the average length of diameters measured at 2 degrees intervals and passing through object's centroid).

For the assessment of the number of macrophages, five 200x randomly selected fields were evaluated.

Results

Results regarding evaluation of both blood and lymphatic vessels are summarized in Table 13.

Tab. 13. Number of blood and lymphatic vessels in the groups of mice.

Group	CD31			LYVE-1		
	number	area	diameter	number	area	diameter
matrigel	5	555	6.1	1.4	28.7	2.6
matrigel with bFGF	26.1	1759	5.8	2.3	63	2.6
Tested compound 0.1 mg/kg Q2X3	9.7	1256	13.5	1	27.7	2
Tested compound 0.1 mg/kg Q1X5	4.6	481	4.8	0.2	4.8	0.5

Macrophagic infiltrate was evaluated within matrigel with bFGF and tested compound administered 0.1 mg/kg Q1X5 groups. Mean values are reported in Table 14 and exemplificative pictures in Figures 16 to 19.

Tab. 14. Mean numbers of macrophages within examined 2 groups.

Group	n°of macrophages	
Matrigel with bFGF	MEAN	16
Matrigel with tested compound 0.1 mg/kg Q1X5	MEAN	8,3

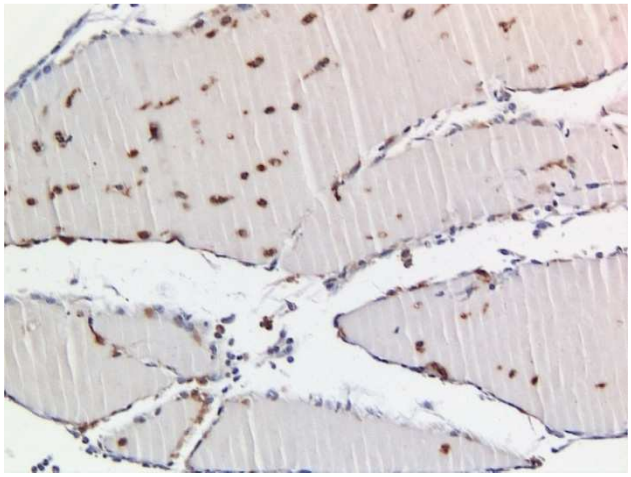

Fig. 16. Matrigel with bFGF, F4/80 IHC, 200x.

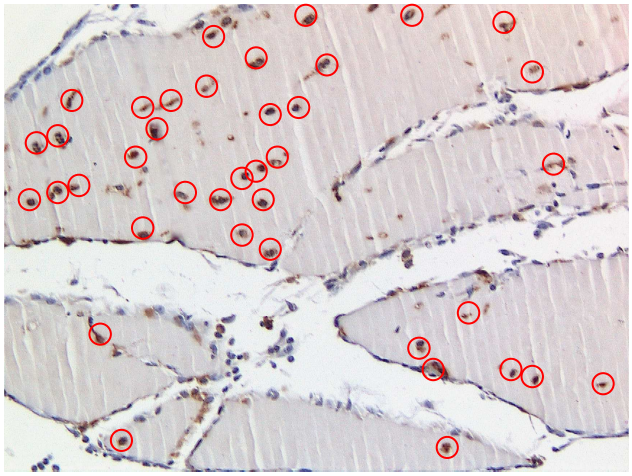

Fig. 17. Matrigel with bFGF, F4/80 IHC, 200x, quantification of macrophagic infiltrate.

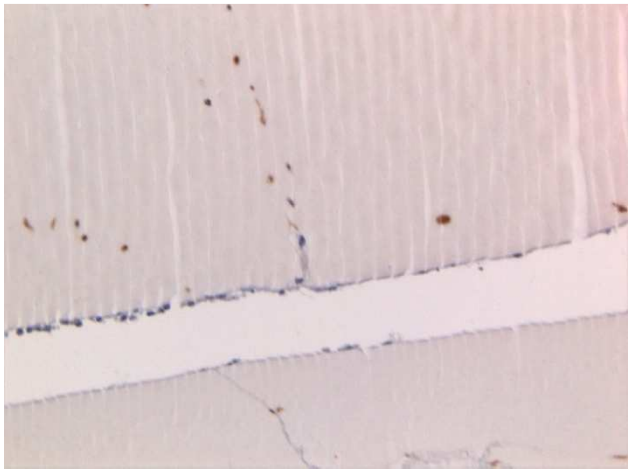

Fig. 18. Matrigel with tested compound 0.1 mg/kg Q1X5, F4/80 IHC, 200x.

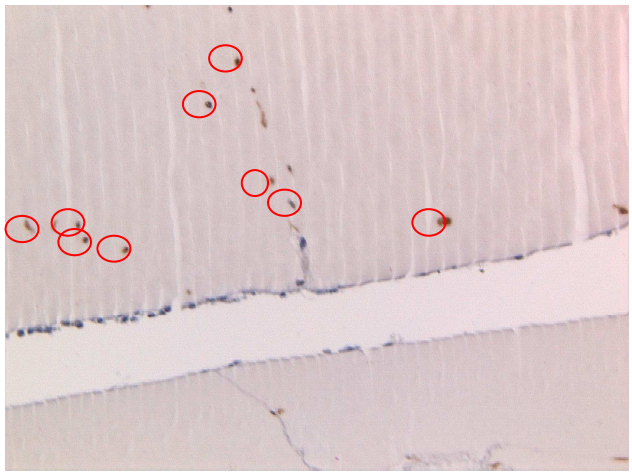

Fig. 19. Matrigel with tested compound 0.1 mg/kg Q1X5, F4/80 IHC, 200x, quantification of macrophagic infiltrate.

Comments

Obtained results mirrored those reported by current literature, with tested compound acting as an antiangiogenic drug (Allavena et al., 2013) and also reducing the number of F4/80-positive macrophages (Germano et al., 2010).

In conclusion, results obtained by this small pivotal study confirmed those reported by current literature and matrigel turned out to be a valid tool.

1.5 -Humane endpoints

There are ethical, scientific and legal reasons for ensuring that adverse effects are minimized in experimental animals. All experiments should incorporate the 3 Rs, as defined by Russell and Burchin in 1959: replacement (of animals with other, non-sentient material or with animals of lower sentience); reduction (of numbers of animals used) and refinement (of technique, “to reduce to an absolute minimum the amount of distress imposed on those animals that are still used”).

In all cases, experimental designs and procedures should be tailored to the needs of the specific studies and a cross-talk between investigators and veterinary pathologists is strongly encouraged, in order to optimize the study set. Furthermore, when possible pilot tumour growth studies using small numbers of animals are recommended. Preliminary data derived from these studies would facilitate the definition of robust and refined endpoints and nowadays imaging techniques available facilitate the development of more defined endpoints for some tumor models.

An “endpoint” is defined as the point at which an experimental animal’s pain and/or distress is terminated, minimized or reduced, by taking actions such as killing the animal humanely, terminating a painful procedure, or giving treatment to relieve pain and/or distress. Early end points reduce non-specific systemic effects and so may increase the precision of the results obtained.

Tumor burden should always be limited to the minimum required for a valid scientific outcome. Assessment of the size of superficial tumors using calipers (usually of two diameters at right angles) is an easy and definable method and calibration curves should be established as part of the characterization of any new tumor system (Workman et al., 1998). For a mouse carrying a single tumor, the mean diameter should not normally exceed 1.2 cm or 1.5 cm for therapeutic studies. Furthermore, scoring of ulceration, distension of covering tissues and cachexia, defined as severe body weight loss, should be incorporated into the endpoints (Workman et al., 2010).

1.6 - Conclusive remarks regarding subcutaneous xenografts

The approach to subcutaneous xenograft starts with a gross evaluation, that can be performed to monitor both successful engraftment of the tumor and tumor growth and animal welfare.

A proper collection of the sample is mandatory and marginal excision should be avoided. Histopathological examination provides useful information about the pattern of tumor growth, cellular morphology, cross-talk between tumor and stroma and intralesional areas of necrosis and inflammation and achieved data can be corroborated by further histochemical and immunohistochemical investigations.

Examples provided above are far from fully elucidate the potential of immunohistochemistry in the characterization of human tumors. Many other antibodies can be profitably used, such as:
-antibodies to characterize tumor cells and get information about the maintenance of their original differentiation (e.g. Vimentin, MyoD1, Desmin, Smooth Muscle Actin and Myoglobin if an original muscular differentiation is under investigation);
-antibodies to characterize the inflammatory infiltrate elicited by tumor growth, taking into account data collected from immunodeficient animals may be underestimated;
-antibodies applied to quantify tumor cell proliferation, such as Ki-67.

A detailed list of the antibodies I used during the PhD period is provided in Table 15.

Tab. 15. Primary antibodies applied in the evaluation of subcutaneous xenografts.

Antigen	Supplier	Clonality	Clone/code n°	Antigen retrieval	Working dilution and detection system	Incubation time	Application
CD31	Dianova	Rat mon	SZ31	HIER	1/50 ABC	1h RT	microvessel number
Smooth muscle actin	LabVision	Rb poly	#RB-9010	HIER	1/50 Alexa	1h RT	microvessel maturity
Cleaved caspase-3	Cell Signaling	Rb poly	Asp175	HIER	1/2500 ABC	1h RT	apoptosis
Ki67	LabVision	Rb mon	#RM-9106-S	HIER	1/400 ABC	1h RT	proliferation
Lyve-1	Abcam	Rb poly	ab14917	HIER	1/200 ABC	1h RT	lymphatic vessels
F4/80	Serotec	Rat mon	Cl:A3-1 MCA497G	digestion	1/150 ABC	1h RT	macrophages

Rat mon: *rat monoclonal*; Rb poly: *rabbit polyclonal*; Rb mon: *rabbit monoclonal*; HIER: *heat-induced epitope retrieval, 0.01 mol/L citrate buffer pH=6.0*; digestion: *enzymatic digestion; Digest-all ^{TM} 3 Pepsin solution RTU (Zymed, S. Francisco, USA);* ABC: *Vector Lab, Vectastain Elite ABC kit PK-6100*; Alexa: Alexa fluor anti-rabbit dye; 1h RT: *one hour at room temperature*

Chapter 2 - Intraperitoneal xenografts

2.1 -Introduction

The evaluation of an intraperitoneal xenograft model is part of a published paper by Oliva et al., 2012 listed in Appendix 1 and an example of a study centered on i.p. evaluation I performed over my 3-year-PhD period is reported below.

Intraperitoneal xenografting is useful in the study of ovarian carcinoma. This approach results in consistent involvement of ovaries and uterus, peritoneal dissemination and production of ascites (Connolly, 2009).

2.2 – Experiment VII- Intraperitoneal xenograft model of human ovarian carcinoma

In collaboration with Istituto Mario Negri of Milan a study on the intraperitoneal (i.p.) dissemination of HOC 22, a human ovarian carcinoma cell line was designed to investigate Bevacizumab combined with chemotherapy on tumor burden.

Epithelial ovarian cancer (EOC) is the leading cause of death for gynecologic malignancy for women in the Western countries mainly because the majority of patients are diagnosed at advanced stage of disease. Advances in early detection, treatment and prevention are required and animal models of ovarian cancer are invaluable tools in these pursuits.

The aim of this study was to evaluate the contributions of chemotherapy (Paclitaxel, PTX + Cisplatin, DDP) and inhibitors of angiogenesis (Bevacizumab, BEV) in controlling spread and progression to secondary organs and ascites formation in the peritoneal cavity of mice injected with a human high-grade serous ovarian carcinoma (HOC 22).

Material and Methods

Six- to eight-week-old female NCr-nu/nu mice were injected with 10 $x10^6$ascites-derived cell suspension of HOC 22 into the peritoneal cavity. Mice were treated with PTX and DDP, singly or in association (PTX + DDP). Bevacizumab was administered according to three protocols: a) in combination with chemotherapy; b) in combination with chemotherapy and continued after the end of the therapy; c) starting 24h after the end of the therapy. Vehicles were administered at the same schedule and route as the active compounds. Three HOC22-bearing mice were necropsied at the beginning of treatment (randomization) to confirm the presence of tumor in the peritoneal cavity. At the end of treatment (interim analysis) four to six mice per group were euthanized and necropsied to establish tumor burden and organs involved in the tumor spread. The remaining mice were also necropsied at the end of the study (survival). A complete necropsy was performed on each mouse and gross findings were recorded and scored (data not shown). Ascites was harvested and the volume was recorded for each mouse (Manenti et al, 2005). For histopathological analysis, organs

(uterus and ovaries, stomach, small intestine, ileocecocolic valve, large intestine, pancreas, kidneys, spleen, liver and gallbladder, diaphragm, heart, lungs and enlarged lymph nodes) were sampled and fixed in 10% neutral buffered formalin. After fixation, tissues were processed and paraffin-embedded and 4-µm sections were stained with hematoxylin and eosin for microscopic examination.

A histological score was used to compare groups. Neoplastic lesions were classified by size as follows:

i. small: up to 10 neoplastic cells;
ii. medium: from 11 to 100 neoplastic cells;
iii. big: more than 100 neoplastic cells.

Up to 10 nodules per size category were counted in each organ and a value of 1 was arbitrarily assigned to each small neoplastic growth, 2 to each medium one and 4 to big ones. Thus, each organ could reach at least 70, except for organs completely effaced by the neoplastic growth, which were arbitrarily assigned a score of 100. A different method was applied to the diaphragm, which was scored according to the percentage of the organ covered by neoplastic cells, as follows:

i. 0%, no neoplastic cells detactable;
ii. 1-25%, assigned a score of 10;
iii. 25-75%, assigned a score of 40;
iv. >75%, assigned a score of 70;
v. >75% with neoplastic cells arranged in several layers or in a nodular mass, assigned a score of 100.

Results

Macroscopically, metastases could be appreciated as whitish nodules as illustrated in Figure 19.

Fig. 19. Example of grossly detectable metastases of HOC 22.

Histologically, HOC 22 metastases were composed of epithelial cells arranged in acini and solid areas, with scant to moderate fibrovascular stroma. Cells were polygonal, 10x50µm in diameter with pale eosinophilic homogeneous cytoplasm and a central nucleus with vesicular chromatin. Mitoses were 4-6 hpf and occasionally atypical. There were intralesional areas of necrosis and

hemorrhage and calcium concrements in acinar lumina (psammoma bodies). Multifocally, clusters of small mature lymphocytes infiltrated the mass.

Necropsy on representative mice showed macroscopic reduction of ascites, but more HOC22 neoplastic aggregates in mice treated with Bevacizumab alone both at interim and killing; reduction of tumor masses was observed after chemotherapy. The liver, ovaries and uterus, diaphragm and pancreas were the organs most commonly involved in tumor dissemination.

Results of the histopathological analysis performed at interim are reported in Table 16 and summarized in Figure 20. Briefly, at interim analysis, the vehicle group had the highest tumor burden and amount of ascites, and mice treated with PTX+DDP+Bev had the lowest ones. The interim analysis indicated that Bevacizumab alone reduces ascites formation (undetectable), but does not limit tumour burden. However, Bevacizumab added to PTX + DDP (PTX + DDP + Bev) reduced both ascites and tumour burden.

Tab.16. Tumor burden and amount of ascites at interim.

	Vehicle	**Bev**	**PTX + DDP**	**PTX + DDP + Bev**
Ascites (ml)	6	/	0,5	/
Tumor burden	15	17	14	14
Most affected organs	ovaries/uterus, **liver**, pancreas, diaphragm, stomach	ovaries/uterus, **liver**, pancreas, lung, kidney, diaphragm, stomach	ovaries/uterus, **liver**, pancreas, diaphragm	**liver**

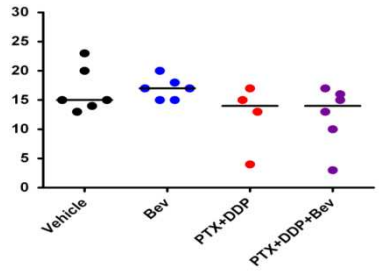

Fig. 20. Tumor burden at interim.

Results of the histopathological analysis performed at killing are reported in Table 17. As expected, tumor scores at killing were higher than those at interim analysis, but with the same pattern. The tumor burden was highest in the Bevacizumab maintenance group, with minimal ascites (not measurable) and a wider range of dissemination than in the other groups.

Tab. 17. Tumor burden and amount of ascites at killing.

	Bev	Bev cont	PTX + DDP	PTX + DDP + Bev	PTX + DDP + Bev cont_stopped	PTX + DDP + Bev cont_maintained
Ascites (ml)	5,5	0,75	7	7	6	5
Tumor burden	20	25	19	16	0	0

Exemplificative pictures are provided in Figures 21 and 22.

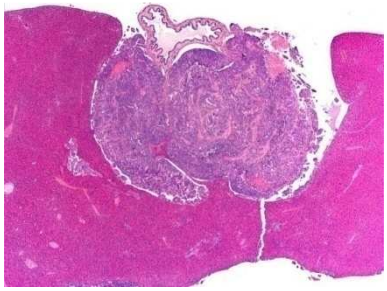

Fig. 21. Note the >100 neoplastic cells metastasis in the mesentery between the liver and the gallbladder and the smaller one in the hepatic parenchyma. HE, 25x

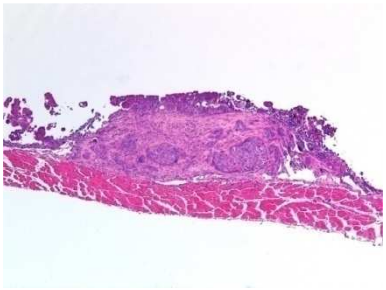

Fig. 22. Massive metastatic invasion of the diaphragm. HE, 50x

Comments

Data achieved from histological analysis closely recapitulated macroscopic findings and highlighted differences among groups in respect of tumor burden and ascites formation. At the doses and schedules used, PTX and DDP single agents were not efficacious, whereas the addition of Bevacizumab significantly prolonged survival for both combinations. Maintenance treatment with Bevacizumab alone inhibited tumour progression and significantly prolonged survival compared with Bevacizumab interrupted after 3 weeks. Only the combination of the two chemotherapeutics with Bevacizumab in maintenance treatment resulted in tumour-free mice. The triple combination (DDP+ PTX + Bev) and maintenance regimens (PTX + DDP + Bev → Bev) were well tolerated, with no clinical signs of toxicity throughout the study or significant body weight loss.

In conclusion, dissemination into the peritoneal cavity is the primary route of progression of ovarian cancer, and ascites and tumour burden correlated with prognosis. These trials indicate an advantage adding Bevacizumab to chemotherapy, which was amplified by a maintenance regimen with Bevacizumab after chemotherapy.

2.3 - Humane endpoints

For tumors growing as a suspension into the peritoneal cavity, it is important to establish clear criteria to ensure that studies are terminated before animal welfare is compromised (Workman et al., 2010). Mice should be monitored twice a week for body weight loss and tumor formation in the peritoneal cavity (abdominal distension) and should be euthanized when they become moribund (Garofalo et al., 2003).

2.4 - Conclusive remarks regarding intraperitoneal xenografts

This site is only appropriate for models where ascites is a feature of the natural progression of the human cancer, e.g. ovarian carcinoma (Workman et al., 2010).

From the HOC 22 study an overall efficacy of Bevacizumab combined with chemotherapy in mouse EOC xenograft models was found. Bevacizumab continued after chemotherapy significantly delayed tumour progression in the peritoneal cavity and prolonged survival. Furthermore, antiangiogenic agents such as Bevacizumab can be administered over long periods with manageable toxicity (Gerber and Ferrara, 2005; Shah et al., 2011). Therefore, it is feasible to use antiangiogenic therapy as a maintenance regimen and it can be expected to prevent or delay cancer recurrence. As already introduced, it is believed that treatments affecting angiogenesis, including bevacizumab, enhance the effect of chemotherapy, by normalizing tumor vasculature, lowering interstitial pressures and improving the delivery of cytotoxic agents (Jain, 2005). Based on these considerations, vascular “normalization” might explain why bevacizumab in combination with chemotherapy was effective in this study.

Chapter 3 -Promising metastatic models

3.1 - Introduction

The metastatic process is critical in modeling cancer because of its clinical relevance and because the majority of human malignant tumors have metastases at the time of diagnosis, either clinically evident or micrometastases (Céspedes et al., 2006). The metastatic process can be regarded as a succession of steps, including invasion of the ECM, intravasation, survival in circulation, adhesion to basement membrane, extravasation, metastatic deposit, angiogenesis and growth. Many mouse models do not develop metastases at all or are scarcely metastastic and in the few spontaneous models available, metastatic deposits may appear only in a limited numbers of sites, with a very long latency (Céspedes et al., 2006).

Metastastic tumors commonly arise within the lung because of the organ's rich capillary network (Harris et al., 2011) that receive the venous blood from all the body.

The evaluation of pulmonary metastases is part of the proceeding production by Castiglioni et al.(2013), listed in Appendix 1 and examples of studies centered on the evaluation of metastases I performed over my 3-year-PhD period are reported below.

3.2 - Experiment VIII- Pulmonary metastases of a subcutaneous xenograft carcinoma

In collaboration with IRCCS, Istituto Nazionale dei Tumori of Milan a promising model of carcinoma metastasizing to the lungs was investigated.

The flank is commonly used for primary xenografts in mice, but it is rare for these tumors to metastasize.

The aim of this study was to develop a reliable spontaneous metastatic murine model with human non-small-cell lung cancer (NSCLC) and to characterize the model as to location of the spontaneously occurring metastases.

Material and Methods

Female SCID mice were injected subcutaneously with NSCLC H460 wt cell line and divided in the following groups of treatment:

-control mice injected with H460 wt;

-mice injected with H460 wt and treated with compound 1 (Cpd 1);

-mice injected with H460 wt and treated with compound 2 (Cpd 2).

Mice were sacrificed at day 45 and lungs were formalin fixed and paraffin embedded. Four µm sections from each lung were routinely stained with Hematoxylin-Eosin (HE) and evaluated under a

light microscope. For a careful examination of metastatic spread to lungs, all lobes of each lung were evaluated. A general description of the metastases was provided and a combined score was set up, considering the number and the size of metastases. According to their size and based on current literature (Sacco et al., 2000), metastases were classified as follows:

-small : < 10 neoplastic cells;
-intermediate: 10-100 neoplastic cells;
-large: >100 neoplastic cells.

Arbitrary, a value of 1 was assigned to each small mass, a value of 2 to each medium mass and a value of 4 to each large one. The evaluation was performed in a blind fashion and only afterwards data were related to corresponding mice.

To confirm the human origin of metastases, selected samples were immunostained with anti-human MHC class I antibody (Abcam), specifically reacting with human tissues and not with murine ones. Furthermore, anti-mouse CD31 (PECAM-1) antibody (Histonova) was also performed, in order to highlight the endothelium of vessels and discriminate between intravascular emboli and metastases.

Results

Multifocally alveolar and perivascular interstitium were expanded by densely cellular, nodular, well demarcated, unencapsulated masses, composed of polygonal cells approximately 15µm in diameter with distinct cell borders, an intermediate N/C ratio and a moderate amount of pale eosinophilic finely granular cytoplasm. Nuclei were 10µm in diameter, oval, with marginated chromatin and an evident paracentral magenta nucleolus. Anisocytosis and anisokaryosis were mild to moderate. There were rare mitoses with bizarre morphology. Occasionally neoplastic cells were detectable within vessels (emboli) and/or are embedded in mats of finely fibrillar to beaded eosinophilic material (fibrin) and in a finely granular eosinophilic material (secretum).
Results of the metastatic count are reported in Table 18.

Tab.18. Number of pulmonary metastases and score assigned.

Group	Sample	N°of small met	N°of intermediate met	N°of large met	score	additional findings
Control H460 wt	#1	0	0	4	**16**	/
	#2	5	5	3	**27**	/
	#3	0	0	1	**4**	/
	#4	1	2	4	**21**	/
	#5	7	4	6	**39**	/
	#6	1	1	0	**3**	/
	mean ± d.s.				**18,3 ± 13,8**	
Cpd 1	#7	0	2	0	**4**	/
	#8	0	2	0	**4**	/
	#9	0	0	0	**0**	/
	#10	1	1	0	**3**	/
	#11	0	1	1	**6**	/
	#12	0	1	1	**6**	/
	mean ± d.s.				**3,8 ± 2,2**	
Cpd 2	#13	1	6	2	**21**	Acidophilic macrophage pneumonia
	#14	6	2	0	**10**	/
	#15	0	1	0	**2**	/
	#16	0	0	0	**0**	/
	#17	2	4	6	**34**	/
	#18	1	6	2	**21**	/
	mean ± d.s.				**14,7 ± 13**	

Mean values are summarized in Table 19 and exemplificative pictures of hematoxylin and eosin and of immunohistochemical markers performed are provided in Figures 23 to 28.

Tab. 19. Sum of mean values of pulmonary metastases.

Group	mean ± d.s.
Control H460 wt	**18,3 ± 13,8**
Cpd 1	**3,8 ± 2,2**
Cpd 2	**14,7 ± 13**

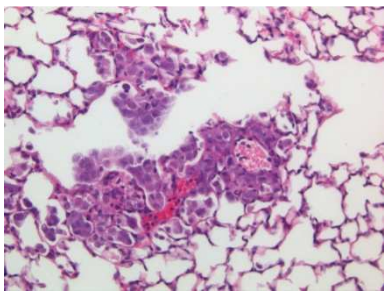

Fig. 23. Crl H460 wt; HE, 20x.

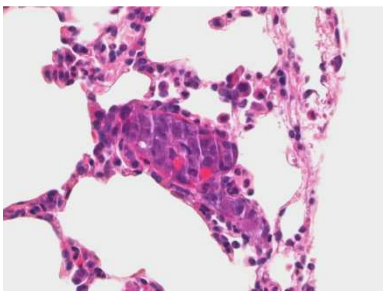

Fig. 24. Crl H460 wt; HE, 40x.

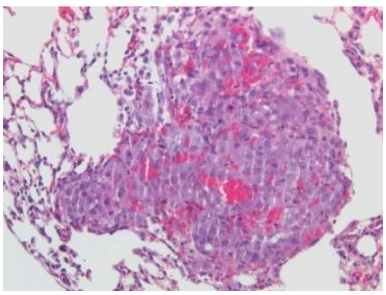

Fig. 25. H460 wt treated with Cpd2; HE, 20x.

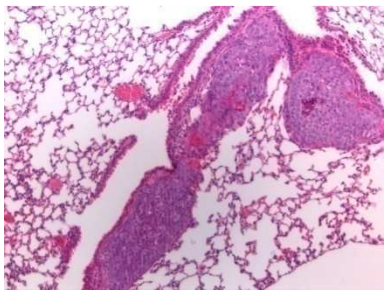

Fig. 26. Crl H460 wt; HE, 10x.

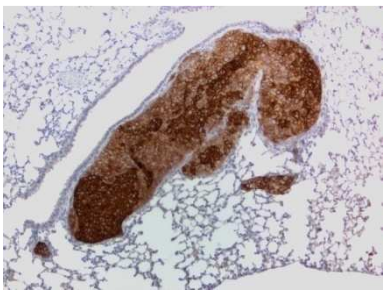

Fig. 27. Crl H460 wt; anti-human MHC class I IHC, 10x.

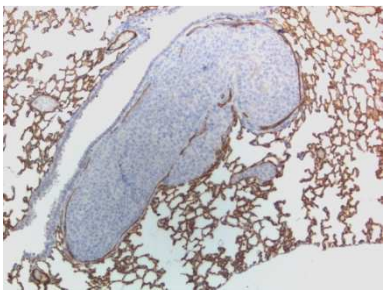

Fig. 28. Crl H460 wt; CD31 IHC, 10x.

Treatment with compound 1 dramatically reduced the number of metastases, whereas results obtained with compound 2 were more variable.

Comments

This study allowed to appreciate the metastatic spreading to the lungs of both tested cell lines. This finding is in contrast with the results reported by Harris et al. (2011) in which no pulmonary spreading was observed with the same cell line implanted subcutaneously in mice at day 49.

The finding of acidophilic macrophage pneumonia (AMP) is an incidental finding, largely described by current literature (Murray and Luz, 1990). Any disease process that impairs normal clearance such as pulmonary tumors as in this case, or Pneumocystosis or other chronic pneumonias can predispose to AMP, that is characterized by the accumulation of acidophilic crystals containing iron, alpha-1 antitrypsin, immunoglobulin and breakdown products of granulocytes within macrophages and alveolar spaces.

Discriminate between intravascular emboli and metastases was not easy in some samples. In general emboli recapitulated the outline of vessels and/or were admixed with erythrocytes. CD31 immunohistochemistry was performed as an attempt to highlight if clusters of neoplastic cells were surrounded by a CD31-positive endothelium (suggestive of an embolus) or not (neoplastic cells already extravasated and thus considered as metastases). In this study emboli were added to metastases. In the majority of cases the endothelium was discontinuous and thus suggestive of an extravasion of neoplastic cells.

The human origin of neoplastic cells was assessed with anti-human MHC class I immunohistochemistry.

In conclusion, the described experimental design is a promising model of a pulmonary metastatic carcinoma.

3.3– Experiment IX- Pulmonary metastases of an intramuscular xenograft sarcoma

In collaboration with IRCCS, Istituto Nazionale dei Tumori of Milan a promising model of an intramuscular sarcoma metastasizing to the lungs was investigated.

The aims of this study were to investigate a promising metastatic sarcoma model and develop an immunohistological method able to detect human disseminated tumor cells in murine lungs.

Material and Methods

Eight SCID mice were injected intramuscularly (IM) or subcutaneously (SC) with 2 or 5 million human A204 rhabdomyosarcoma cells and euthanized after 9 weeks. Lungs were formalin-fixed, paraffin-embedded, sectioned at 4 µm and stained with Hematoxylin and Eosin (HE) for routine histopathological examination. Immunohistochemistry (IHC) and immunofluorescence (IF) were performed on serial sections for the assessment of tumor cell dissemination to the lung using specific anti-human antibodies, i.e. anti-Vimentin clone sp20 (reported to specifically react with human mesenchymal cells) and anti-human MHC class I antibodies. Image analysis was performed on Vimentin sp20-stained sections. The number of positive neoplastic cells was counted using ImageJ analysis program (http://rsb.info.nih.gov/ij/) in six 400x microscopic fields selected within the areas with strongest signal (hot spot fields). Double-immunofluorescence was performed to assess if the two markers colocalized. Double immunofluorescently labeled sections were acquired with the Leica TCS SPE confocal microscope (Leica Microsystems GmbH, Wetzlar, Germany). The fluorophores (Alexa Fluor® 555 Goat Anti-Rabbit IgG (H+L), Molecular Probes® and Alexa Fluor® 488 Goat Anti-Rabbit IgG (H+L), Molecular Probes®) were excited with the 488 nm and the 532 nm laser lines and the emitted fluorescence acquired in sequential scan mode with ACS APO 10x/0.3 Dry and ACS APO 40x/1.15 Oil CS objectives. Nuclei were visualized by DAPI staining (405 nm laser line excitation).

Results

Detection of neoplastic cells within pulmonary interstitium in HE stained sections was very challenging and hampered by the fact that suspected neoplastic cells were closely intermingled with murine cells and were not arranged in aggregates recapitulating primary muscular tumor. IHC performed on serial sections with anti-Vimentin and anti-human MHC class I antibodies allowed to appreciate atypical cells arranged either singly or in small clusters infiltrating pulmonary interstitium (Fig. 29 and Fig. 31 and Fig. 30 and Fig. 32, respectively). A blind quantification of the cells resulted in a higher number of human neoplastic cells in the lung of mice injected with 5 million cells rather than of mice injected with 2 million cells. The mouse injected subcutaneously had the lowest numbers of pulmonary metastases, as reported in Table 19.

Tab. 19. Results of metastatic evaluation based on Vimsp20 immunohistochemistry.

Group	Sample	field a	field b	field c	field d	field e	field f	tot	mean
IM - 2 million A204 cells	#1	10	7	12	15	9	9	62	10,3
	#2	14	18	6	3	23	5	69	11,5
	#3	13	3	26	30	8	21	101	16,8
	#4	11	3	9	4	7	6	40	6,7
	tot							**272**	**11,3**
IM- 5 million A204 cells	#5	38	56	25	23	30	18	190	31,7
	#6	29	14	10	11	22	6	92	15,3
	#7	10	15	17	17	15	12	86	14,3
	tot							**368**	**20,4**
SC - 5 million A204 cells	#8	1	1	4	1	3	4	**14**	**2,3**

These results were confirmed by anti-human MHC class I immunohistochemistry and although the immunolabeling of this antibody was fainter than that observed with Vimentin sp20, obtained results mirrored those achieved with Vimentin alone.

Representative pictures are provided in Figure 29 to 32.

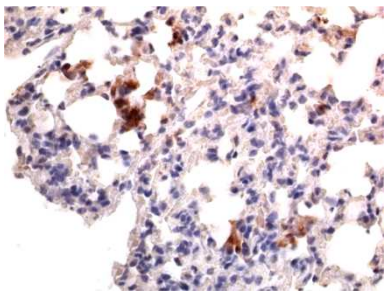

Fig. 29. Randomly selected field, sample #1. MHC I IHC, 400x.

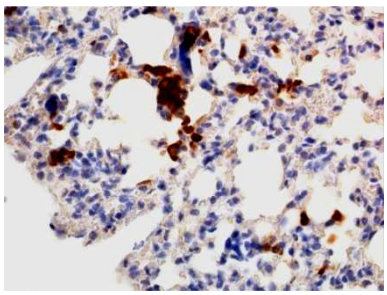

Fig. 30. Randomly selected field, sample #1. Vimentin IHC, 400x.

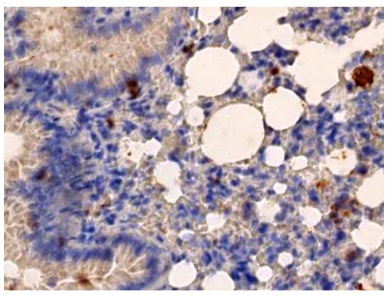

Fig. 31. Randomly selected field, sample #1. MHC I IHC, 400x.

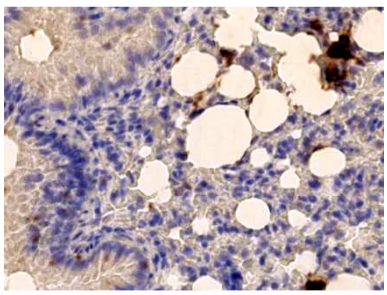

Fig. 32. Randomly selected field, sample #1. Vimentin IHC, 400x.

To evaluate the specificity of both markers to detect exclusively human tissues, sections from either non pathological murine lungs and from lungs with inflammatory lesions were immunostained with both Vimentin and anti-human MHC class I.

No specific immunoreactivity was observed, with only a minimal background signal on bronchiolar epithelium. Exemplificative pictures are provided in Figures 33 to 35.

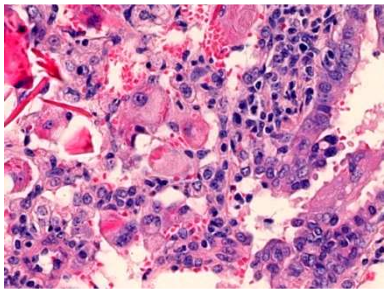

Fig. 33. Focus of histiocytic pneumonia, with intralesional crystals. HE, 400x.

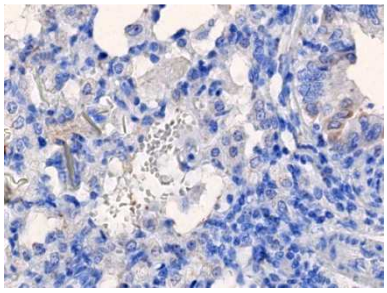

Fig. 34. Serial section of Fig. 32. No specific immunoreactivity observed. Anti-human MHC class I IHC, 400x.

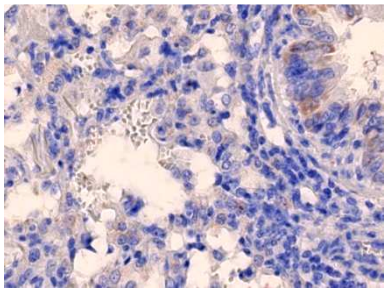

Fig. 35. Serial section of Fig. 32. No specific immunoreactivity observed. Vimentin sp20 IHC, 400x.

As a final step, double-immunofluorescence assessed the two markers colocalized in the same atypical cells. Exemplificative pictures are provided in Figures 36 to 38.

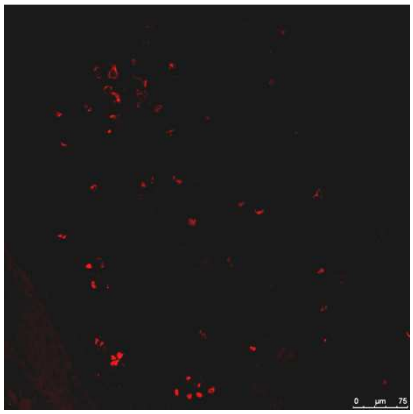

Fig. 36. Disseminated tumor cells infiltrating pulmonary interstitium were immunofluorescently labelled by Vimentin. IF staining, confocal, scale bar 50µm.

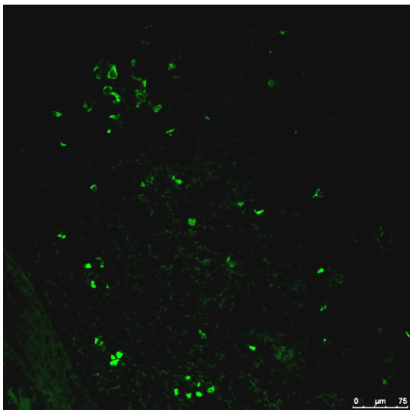

Fig. 37. Disseminated tumor cells infiltrating pulmonary interstitium were immunofluorescently labelled by MHC I. IF staining, confocal, scale bar 50µm.

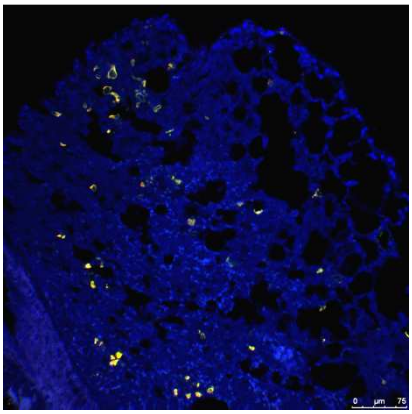

Fig. 38. Both markers co-localized in the same atypical cells (yellow) (c and d), thus demonstrating that these cells were of mesenchymal and human origin. Vimentin, MHC I and DAPI signal shown.

Comments

This experiment confirmed that rabbit monoclonal anti-Vimentin clone SP20 (Labvision) holds a species-specificity for human mesenchymal cells as stated by the Manufacturer's datasheet, since it does not immunolabel FFPE murine tissues. Anti-human MHC class I and Vimentin sp20 are useful markers in the detection of human mesenchymal cells and do not cross-react with murine tissue.

In conclusion, intramuscular injection of A204 rhabdomyosarcoma cells can be regarded as a valuable metastatic orthotopic xenograft model. Immunohistological methods using specific anti-human antibodies are a reliable tool for the detection of disseminated xenografted tumor cells.

3.4 - Conclusive remarks regarding xenograft metastatic models

Pulmonary metastases can occasionally be detected grossly with the aid of a stereomicroscope. In the majority of cases, a careful histological evaluation is mandatory and allows to detect small clusters of neoplastic cells. In other cases, the detection of metastases is even more challenging and an immunohistological approach is required to discriminate between human metastatic neoplastic cells and interstitial stroma.

Conclusions

Animal models are essential in the study of human malignancies and have a great potential for further improvement. In general, the ideal animal model should recapitulate pathogenesis and histopathological features, elicit physiological and systemic effects and involve the same genetic and biochemical pathways of the human counterpart (Céspedes et al., 2006). In light of these considerations, xenografts mouse models are a valuable and promising tool and have been extensively used in the study of human malignancies. Nevertheless, there is a lack of standardization in current literature, with no detailed guidelines for their sampling and evaluation provided so far.

This report aimed at describing a straightforward approach to this model through histopathological and immunohistochemical analyses. I would like to stress that these evaluations are complementary and not alternative to *in vitro* analyses and to other evaluations carried on live mice, such as the collection of parameters from murine serum, urine, etc. and/or imaging techniques. Among these latter, bioluminescence imaging (BLI) has recently emerged as a valid method for rapid, cheap, facile screening of tumor growth and spread in mice. BLI can be profitably applied to both subcutaneous and orthotopic tumor models with high sensitivity and reproducibility and it is used for assessing chemotherapeutic efficacy, drug combinations, dosing and timing (Contero et al., 2009).

A combined approach and a strict cooperation between *in vivo* operators such as biologists and technicians and veterinary pathologists both in the set up of experimental protocols and in animal monitoring is thus strongly encouraged in order to maximize the amount of data that can be collected from sacrificed animals, to optimize the collection of samples and finally to improve the quality of scientific data obtained. Furthermore, the veterinary pathologist should be able to provide information regarding animal welfare, which is a topic of debate nowadays, raising several ethical concerns.

As an attempt to bypass this problem, alternative models eliciting less ethical concerns have recently flourished, such as the use of zebrafish. Both adult and juvenile zebrafish (*Danio rerio*) represent in fact a promising alternative model in cancer research (Lam et al., 2006), with peculiar emphasis on vascular biology studies. Zebrafish spontaneously develops almost any type of tumor, most commonly in testis, gut, thyroid, liver, peripheral nerve, connective tissue and ultimobranchial gland and over the past few years, human tumor cell transplantation into zebrafish has developed (Lee et al., 2005), later optimized with prevention of rejection obtained by dexamethasone administration (Stoletov et al., 2007) or sublethal γ irradiation (White et al., 2008). Despite evaluable points of strength such as the possibility to visualize tumor cell, zebrafish model has lots

of weak points, first of all the difference in temperature requirement of human vs piscine cells and cellular size, with zebrafish vessels and other anatomical structures smaller than the corresponding human structures. Overall, although zebrafish are a useful model, there is evidence they won't supplant the use of mammalian model system such as the mouse.

Genetically engineered mouse (GEM) models are an additional strategy allowing to bypass several of the weak points depicted for human tumor xenografts. A genetically modified mouse is a mouse that has had its genome altered through the use of genetic engineering techniques, so that one or more genes thought to be involved in transformation or malignancy are mutated, deleted or overexpressed (Richmond and Su, 2008). Briefly, the major advantages with GEM are that these mice are immunocompetent, so that tumor microenvironment can mirror the human counterpart and that specific genetic abnormalities that are present in human tumors can be reproduced in an inducible manner, at specific ages and in the tissue-type or origin (conditional knockout).

Finally, it should be mentioned that pet dogs and cats can be regarded as well as valid model tumor systems. The pet population develops spontaneous tumors with histopathologic and biologic behavior similar to tumors occurring in humans, thus this underutilized resource that has the advantage to lack ethical implications can provide insights into the study of human malignancies (MacEwen, 1990; Ranieri et al., 2013).

Overall, all models have strengths and limitations and despite weak points, ethical concerns and limitations, animal models will never be completely replaced by *in vitro* approaches that are poorly predictive of the behaviour of the complex system represented by the whole organism.

Acknowledgements

I wish to express my gratitude to all those Colleagues from the following institutions that contributed to this project:

- laboratory “Biologia e Terapia delle Metastasi Tumorali”- Dr.ssa Raffaella Giavazzi and her Group, Department of Oncology, Mario Negri Institute for Pharmacological Research, Milan, Italy;
- laboratory “Angiogenesi tumorale”- Dr.ssa Giulia Taraboletti and her Group, Department of Oncology, Mario Negri Institute for Pharmacological Research, Bergamo, Italy;
- Molecular Pharmacology Unit- Dr.ssa Cinzia Lanzi and her Group, Department of Experimental Oncology and Molecular Medicine, Fondazione IRCCS Istituto Nazionale dei Tumori, Milan, Italy;
- Molecular Pharmacology Unit- Dr.ssa Paola Perego and her Group, Department of Experimental Oncology and Molecular Medicine, Fondazione IRCCS Istituto Nazionale dei Tumori, Milan, Italy;

References

- Achen MG, Jeltsch M, Kukk E, Mäkinen T, Vitali A, Wilks AF, Alitalo K, Stacker SA. Vascular endothelial growth factor D (VEGF-D) is a ligand for the tyrosine kinases VEGF receptor 2 (Flk1) and VEGF receptor 3 (Flt4). *Proc Natl Acad Sci* U S A. 1998 Jan 20;95(2):548-53.
- Alitalo K, Carmeliet P. Molecular mechanisms of lymphangiogenesis in health and disease. *Int J Cancer*. 2002; 123: 219-227.
- Allavena P, Germano G, Belgiovine C, D'Incalci M, Mantovani A. Trabectedin: A drug from the sea that strikes tumor-associated macrophages. *Oncoimmunology*. 2013; 2(6):e24614.
- Baluk P, Hashizume H, McDonald DM. Cellular abnormalities of blood vessels as targets in cancer. *Curr Opin Genet Dev*. 2005; 15: 102-111.
- Breiteneder-Geleff S, Soleiman A, Kowalski H, Horvat R, Amann G, Kriehuber E, Diem K, Weninger W, Tschachler E, Alitalo K, Kerjaschki D. Angiosarcomas express mixed endothelial phenotypes of blood and lymphatic capillaries: podoplanin as a specific marker for lymphatic endothelium. *Am J Pathol.* 1999 Feb;154(2):385-94.
- Céspedes MV, Casanova I, Parreno M, Mangues R. Mouse models in oncogenesis and cancer therapy. *Clin Transl Oncol*. 2006; 8: 318-329.
- Connolly DC. Animal models of ovarian cancer. *Cancer Treat Res*. 2009; 149: 353-391.
- Contero A, Richer E, Gondim A, Mason RP. High-throughput quantitative bioluminescence imaging for assessing tumor burden.*Methods Mol Biol*. 2009; 574: 37-45.
- Dawson DW, Pearce SF, Zhong R, Silverstein RL, Frazier WA, Bouck NP. CD36 mediates the in vitro inhibitory effects of thrombospondin-1 on endothelial cells. J Cell Biol. 1997; 138: 707-717.
- Díaz-Flores L, Gutiérrez R, Varela H, Rancel N, Valladares F. Microvascular pericytes: a review of their morphological and functional characteristics. *Histol Histopathol*. 1991; 6 (2): 269-286.
- Dickson PV, Hamner JB, Sims TL, Fraga CH, Ng CY, Rajasekeran S, Hagedorn NL, McCarville MB, Stewart CF, Davidoff AM. Bevacizumab-induced transient remodeling of the vasculature in neuroblastoma xenografts results in improved delivery and efficacy of systemically administered chemotherapy. *Clin Cancer Res*. 2007; 13: 3942-3950.
- Ebata N, Nodasaka Y, Sawa Y, Yamaoka Y, Makino S, Totsuka Y, Yoshida S. Desmoplakin as a specific marker of lymphatic vessels. *Microvasc Res*. 2001 Jan;61(1):40-8.
- Folkman J. Fundamental concepts of the angiogenic process. *Curr Mol Med.* 2003; 3: 643-651.
- Folkman J. Angiogenesis: an organization princible for drug discovery? *Nat Rev Drug Discov.* 2007; 6: 273-286.
- Foreman O, Kavirayani AM, Griffey SM, Reader R, Shultz LD. Opportunistic bacterial infections in breeding colonies of the NSG mouse strain. *Vet Pathol*. 2011; 48 (2): 495-499.

- Fulzele SV, Chatterjee A, Shaik MS, Jackson T, Singh M. Inhalation delivery and anti-tumor activity of celocoxib in human orthotopic non-small cell lung cancer xenograft model. Pharm Res. 2006. 23: 2094-2106.
- Garofalo A, Naumova E, Manenti L, Ghilardi C, Ghisleni G, Caniatti M, Colombo T, Cherrington JM, Scanziani E, Nicoletti MI, Giavazzi R. The combination of the tyrosine kinase receptor inhibitor SU6668 with paclitaxel affects ascites formation and tumor spread in ovarian carcinoma xenografts growing orthotopically. *Clin Cancer Res*. 2003. 9: 3476-85
- Gasparini G, Longo R, Fanelli M, Teicher BA. Combination of antiangiogenic therapy with other anticancer terapie: results, challenges, and open questions. *J Clin Oncol*. 2005. 23: 1295-1311.
- Gerber HP, Ferrara N. Pharmacology and pharmacodynamics of bevacizumab as monotherapy or in combination with cytotoxic therapy in preclinical studies. *Cancer Res*. 2005. 65: 671-680.
- Gerhardt H and Betsholtz C. Endothelial-pericyte interactions in angiogenesis. *Cell Tissue Res*. 2003. 314 (1): 15-23.
- Germano G, Frapolli R, Simone M, Tavecchio M, Erba E, Pesce S, Pasqualini F, Grosso F, Sanfilippo R, Casali PG, Gronchi A, Virdis E, Tarantino E, Pilotti S, Greco A, Nebuloni M, Galmarini CM, Tercero JC, Mantovani A, D'Incalci M, Allavena P. Antitumor and anti-inflammatory effects of Trabectedin on human myxoid liposarcoma cells. *Cancer Res*. 2010; 70(6): 2235-2244.
- Goel S, Duda DG, Xu L, Munn LL, Boucher Y, Fukumura D, Jain RK. Normalization of the vasculature for treatment of cancer and other diseases. *Physiol Rev*. 2011; 91(3): 1071-1121.
- Griffioen AW, Mans LA, de Graaf AM, Nowak-Sliwinska P, de Hoog CL, de Jong TA, Vyth-Dreese FA, van Bejinum JR, Bex A, Jonasch E. Rapid angiogenesis onset after discontinuation of sunitinib treatment of renal cell carcinoma patients. *Clin Cancer Res*. 2012; 18(14): 3961-3971.
- Hagendoorn J, Tong R, Fukumura D, Lin Q, Lobo J, Padera TP, Xu L, Kucherlapati R, Jain RK. Onset of abnormal blood and lymphatic vessel function and interstitial hypertension in early stages of carcinogenesis. *Cancer Res*. 2006; 66: 3360-3364.
- Hanahan D, Weinberg RA. Hallmarks of cancer: the next generation. *Cell*. 2011; 144: 646-674.
- Harris JE, Shin J, Lee B, Pelosky K, Hooker CM, Harbom K, Hulbert A, Zahnow C, Yang SC, Baylin S, Brayton C, Brock MV. A murine xenograft model of spontaneous metastases of human lung adenocarcinoma. *J Surg Res*. 2011; 171(1): e75-e79.
- Hasan J, Byers R, Jayson GC. Intra-tumoural microvessel density in human solid tumours. *British J of Cancer*. 2002; 86: 1566-1577.
- Hirschi KK and D'Amore PA. Pericytes in the microvasculature. *Cardiovascular Research*. 1996: 687-698.
- Jain RK. Normalization of tumor vasculature: an emerging concept in antiangiogenic therapy. *Science*. 2005. 307: 58-62.

- Jackson DG, Prevo R, Clasper S, Banerji S. LYVE-1, the lymphatic system and tumor lymphangiogenesis. *Trends Immunol*. 2001 Jun;22(6):317-21.
- Jin K, Teng L, Shen Y, He K, Xu Z and Li G. Patient-derived human tumour tissue xenografts in immunodeficient mice: a systematic review. *Clin Transl Oncol*. 2010; 12: 473-480.
- Joukov V, Pajusola K, Kaipainen A, Chilov D, Lahtinen I, Kukk E, Saksela O, Kalkkinen N, Alitalo K. A novel vascular endothelial growth factor, VEGF-C, is a ligand for the Flt4 (VEGFR-3) and KDR (VEGFR-2) receptor tyrosine kinases. *EMBO J*. 1996 Jan 15;15(2):290-98.
- Kaipainen A, Korhonen J, Mustonen T, van Hinsbergh VW, Fang GH, Dumont D, Breitman M, Alitalo K. Expression of the fms-like tyrosine kinase 4 gene becomes restricted to lymphatic endothelium during development. *Proc Natl Acad Sci* U S A. 1995 Apr 11;92(8):3566-70.
- Kavirayani AM, Foreman O. Retrospective study of spontaneous osteosarcomas in the nonobese diabetic strain and nonobese diabetic-derived substrains of mice. *Vet Pathol*. 2010; 47 (3): 482-487.
- Konantz M, Balci TB, Hartwig UF, Dellaire G, André MC, Berman JN, Lengerke C. Zebrafish xenografts as a tool for in vivo studies on human cancer. *Ann N Y Acad Sci*. 2012; 124-137.
- Lam SH, Wu YL, Vega VB, Miller LD, Spitsbergen J, Tong Y, Zhan H, Govindarajan KR, Lee S, Mathavan S, et al. Conservation of gene expression signatures between zebrafish and human liver tumors and tumor progression. *Nat Biotechnol*. 2006; 24: 73-75.
- MacEwen EG. Spontaneous tumors in dogs and cats: models for the study of cancer biology and treatment. Cancer Metastasis Rev 1990; 9(2): 125-136.
- Manenti L, Riccardi E, Marchini S, Naumova E, Floriani I, Garofalo A, Dossi R, Marrazzo E, Ribatti D, Scanziani E, Bani M, Belotti D, Broggini M, Giavazzi R. Circulating plasma vascular endothelial growth factor in mice bearing human ovarian carcinoma xenograft correlates with tumor progression and response to therapy. *Mol Cancer Ther* 2005. 4: 715-25.
- Matson DR, Stukenberg PT. Spindle poisons and cell fate: a tale of two pathways. Mol Interventions. 2011; 11(2): 141-150.
- McDonald DM and Choyke PL. Imaging of angiogenesis: from microscope to clinic. Nat Med. 2003; 9: 713-725.
- Morton CL and Houghton PJ. Establishment of human tumor xenografts in immunodeficient mice. Nat Protocols. 2007; 2(2): 247-250.
- Muruganandham M, Lupu M, Dyke JP, Matei C, Linn M, Packman K, Kolinsky K, Higgins B, Koutcher JA. Preclinical evaluation of tumor microvascular response to a novel antiangiogenic/antitumor agent RO0281501 by dynamic contrast-enhanced MRI at 1.5 T. *Mol Cancer Ther*. 2006; 5: 1950-1957.
- Nadir Y, Brenner B. Heparanase coagulation and cancer progression. *Best Pract Res Clin Haematol*. 2009; 22(1): 85-92.

- Nicolini V, Cassinelli G, Cuccuru G, Bongarzone I, Petrangolini G, Tortoreto M, Mondellini P, Casalini P, Favini E, Zaffaroni N, Zunino F, Lanzi C. Interplay between Ret and Fap-1 regulates CD95-mediated apoptosis in medullary thyroid cancer cells. *Biochem Pharmacol*. 2011; 82(7): 778-788.
- Passaniti A, Taylor RM, Pili R, Guo Y, Long PV, Haney JA, Pauly RR, Grant DS, Martin GR. A simple, quantitative method for assessing angiogenesis and antiangiogenic agents using reconstituted basement membrane, heparin, and fibroblast growth factor. *Lab Invest* 1992; 67(4): 519-528.
- Portugal J, Mansilla S, Bataller M. Mechanisms of drug-induced mitotic catastrophe in cancer cells. *Current Pharmaceutical Design*. 2010; 16: 69-78.
- Ragel BT, Jensen RL, Gillespie DL, Prescott SM, Couldwell WT. Celocoxib inhibits meningioma tumor growth in a mouse xenograft model. *Cancer*. 2007; 109: 588-597.
- Ranieri G, Gadaleta CD, Patruno R, Zizzo N, Daidone MG, Hansson MG, Paradiso A, Ribatti D. A model of study for human cancer: Spontaneous occurring tumors in dogs. Biological features and translation for new anticancer therapies.*Crit Rev Oncol Hematol*. 2013; 88(1):187-97.
- Richmond A and Su Y. Mouse xenograft models vs GEM models for human cancer therapeutics. *Disease Models & Mechanisms*. 2008; 1: 78-82.
- Roninson IB, Broude EV, Chang BD. If not apoptosis, then what? Treatment-induced senescence and mitotic catastrophe in tumor cells. *Drug Res Update*. 2001; 4: 303-313.
- Russell WMS, Burch RL. The principles of humane experimental technique, Kindon: Methuen. 238 pp. 1959. Universities Federation for Animal Welfare (UFAW), Potters Bar, Herts, UK: England. Special edition (1992).
- Sacco MG, Caniatti M, Catò EM, Frattini A, Chiesa G, Ceruti R, Adorni F, Zecca L, Scanziani E, Vezzoni P. Liposome-derived angiostatin strongly inhibits tumor growth and metastatization in a transgenic model of spontaneous breast cancer. *Cancer Res*. 2000; 60(10): 2660-5.
- Shah DK, Veith J, Bernacki RJ, Balthasar JP. Evaluation of combined bevacizumab and intraperitoneal carboplatin or paclitaxel therapy in a mouse model of ovarian cancer. *Cancer Chemother Pharmacol*. 2011. 68: 951-958.
- Stoletov K, Montel V, Lester RD, Gonias SL, Klemke R. High-resolution imaging of the dynamic tumor cell vascular interface in transparent zebrafish. *Proc Natl Acad Sci*. 2007; 104: 17406-17411.
- Thorpe PE. Vascular targeting agents as cancer therapeutics. *Clin Cancer Res*. 2004; 10: 415-427.
- Tobia C, De Sena G, Presta M. Zebrafish embryo, a tool to study tumor angiogenesis. *Int J Dev Biol*. 2011; 55: 505-509.

- Tong RT, Boucher Y, Kozin SV, Winkler F, Hicklin DJ, Jain RK. Vascular normalization by vascular endothelial growth factor receptor 2 blockade induces a pressure gradient across the vasculature and improves drug penetration in tumors. *Cancer Res*. 2004; 64: 3731-3736.
- Vanzulli S, Gazzaniga S, Braidot MF, Vecchi A, Mantovani A, Wainstok de Calmanovici R. Detection of endothelial cells by MEC 13.3 monoclonal antibody in mice mammary tumors. *Biocell*. 1997; 21: 39-46.
- Volk LD, Flister MJ, Bivens CM, Stutzman A, Desai N, Trieu V, Ran S. Nab-paclitaxel efficacy in the orthotopic model of human breast cancer is significantly enhanced by concurrent anti-vascular endothelila growth factor A therapy. *Neoplasia*. 2008; 10: 613-623.
- Wang D, Stockard CR, Harkins L, Lott P, Salih C, Yuan K, Buchsbaum D, Hashim A, Zayzafoon M, Hardy R, Hameed O, Grizzle W, Siegal GP. Immunohistochemistry for the evaluation of angiogenesis in tumor xenografts. *Biotech histochem*. 2008; 83(3); 179-189.
- White RM, Sessa A, Burke C, Bowman T, Leblanc J, Ceol C, Bourque C, Dovey M, Goessling W, Burns CE et al. Transparent adult zebrafish as a tool for *in vivo* transplantation analysis. *Cell Stem Cell*. 2008; 2: 183-189.
- Wildiers H, Guetens G, De Boeck G, Verbeken E, Landuyt B, Landuyt W, de Bruijn EA, van Oosterom AT. Effect of antivascular endothelial growth factor treatment on the intratumoral uptake of CPT-11. *Br J Cancer*. 2003; 88: 1979-1986.
- Wingle JT, Oliver G. Prox1 Function Is Required for the Development of the Murine Lymphatic System. *Cell*. 1999; 98 (6): 769-778.
- Winkler F, Kozin SV, Tong RT, Chae SS, Booth MF, Garkavtsev I, Xu L, Hicklin DJ, Fukumura D, di Tomaso E, et al. Kinetics of vascular normalization by VEGFR2 blockade governs brain tumor response to radiation: role of oxygenation, angiopoietin-1, and matrix metalloproteinases. *Cancer Cell*. 2004; 6: 553-563.
- Workman P, Twentyman P, Balkwill F, et al. United Kingdom Coordinatin Committee on Cancer Research (UKCCCR) Guidelines for the welfare of animals in experimental neoplasia (Second Edition, July 1997). 1998. *Br J of Cancer* 77: 1-10.
- Workman P, Aboargye EO, Balkwill F, Balmain A, Bruder G, Chaplin DJ, Double JA, Everitt J, Farningham DAH, Glennie MJ, Kelland LR, Robinson V, Stratford IJ, Tozer GM, Watson S, Wedge SR, Eccles SA. Guidelines for the welfare and use of animals in cancer research. 2010.*Br J Cancer* 102, 1555-1577.
- Yu JL, Coomber BL, Kerbel RS. A paradigm for therapy-induced microenvironmental changes in solid tumors leading to drug resistance. *Differentiation*. 2002; 70: 599-609.

Appendix 1 List of the scientific publications that include the contribution of the approach to human xenografts developed in this work.

***Mol Cancer Ther*. 2013 Oct;12(10):2237-47.**

Chemotherapy counteracts metastatic dissemination induced by antiangiogenic treatment in mice.Rovida A, **Castiglioni V**, Decio A, Scarlato V, Scanziani E, Giavazzi R, Cesca M.

The development of resistance and progressive disease after treatment with angiogenesis inhibitors is becoming a controversial issue. We investigated the experimental conditions that cause multireceptor tyrosine kinase inhibitors (RTKI) to augment metastasis and whether opportune combinations with chemotherapy could counteract this effect. The renal Renca-luc tumor was transplanted orthotopically in the kidney of Balb/c mice, which then were or were not nephrectomized. The Lewis Lung carcinoma (LLC) was transplanted in the tibial muscle of C57/Bl6 mice. Treatment with the RTKI sunitinib started at different stages of tumor progression, mimicking neoadjuvant or adjuvant settings. Combination studies with paclitaxel, doxorubicin, cisplatin, gemcitabine, and topotecan were done on the LLC model, using opportune regimens. In a neoadjuvant setting, sunitinib inhibited Renca-luc tumor growth, prolonging survival despite an increase in lung metastasis; treatment after primary tumor surgery (adjuvant setting) or on established metastasis prolonged survival and decreased metastasis. Sunitinib increased lung metastasis from mice bearing early-stage LLC, but did not affect established metastases (no acceleration) from advanced tumors. Combinations with doxorubicin ,topotecan, gemcitabine, but not cisplatin and paclitaxel, counteracted the increase in metastasis from LLC, partly reflecting their antitumor activity. Histology analysis after sunitinib confirmed tumor vascular changes and increased hypoxia. Topotecan at suboptimal daily doses reduced sunitinib-related metastasis, reducing tumor hypoxia. Tyrosine kinase inhibitors, as sunitinib, can have adverse malignant effects mainly in the neoadjuvant setting. The addition of chemotherapy might influence metastasis, depending on each drug mechanism of action and its regimen of administration.

***J Med Chem*. 2012 Dec 13;55(23):10460-74.**

Synthesis and biological evaluation (in vitro and in vivo) of cyclic arginine-glycine-aspartate (RGD) peptidomimetic-paclitaxel conjugates targeting integrin αVβ3.

Colombo R, Mingozzi M, Belvisi L, Arosio D, Piarulli U, Carenini N, Perego P, Zaffaroni N, De Cesare M, **Castiglioni V**, Scanziani E, Gennari C.

A small library of integrin ligand−paclitaxel conjugates 10−13 was synthesized with the aim of using the tumor-homing cyclo[DKP-RGD]peptidomimetics for site-directed delivery of the cytotoxic drug. All the paclitaxel−RGD constructs 10−13 inhibited biotinylated vitronectin binding to the purified αVβ3 integrin receptor at low nanomolar concentration and showed in vitro cytotoxic activity against a panel of human tumor cell lines similar to that of paclitaxel. Among the cell lines, the cisplatin-resistant IGROV-1/Pt1 cells expressed high levels of integrin αVβ3, making them attractive to be tested in *in vivo* models. cyclo[DKP-f 3-RGD]-PTX 11 displayed sufficient stability in physiological solution and in both human and murine plasma to be a good candidate for in vivo testing. In tumor-targeting experiments against theIGROV-1/Pt1 human ovarian carcinoma xenotransplanted in nude mice, compound 11 exhibited a superior activity compared with paclitaxel, despite the lower (about half) molar dosage used.

***BioconjugChem*. 2012 Aug 15;23(8):1610-22.**

Design, synthesis, and biological evaluation of novel cRGD-paclitaxel conjugates for integrin-assisted drug delivery.

Pilkington-Miksa M, Arosio D, Battistini L, Belvisi L, De Matteo M, Vasile F, Burreddu P, Carta P, Rassu G, Perego P, Carenini N, Zunino F, De Cesare M, **Castiglioni V**, Scanziani E, Scolastico C, Casiraghi G, Zanardi F, Manzoni L.

The efficacy of taxane-based antitumor therapy is limited by several drawbacks which result in a poor therapeutic index. Thus, the development of approaches that favor selective delivery of taxane drugs (e.g., paclitaxel, PTX)to the disease area represents a truly challenging goal. On the basis of the strategic role of integrins in tumor cell survival and tumor progression, as well as on integrin expression in tumors, novel molecular conjugates were prepared where PTX is covalently attached to either cyclic AbaRGD (Azabicycloalkane-RGD) or AmproRGD (Aminoproline-RGD) integrin recognizing matrices via structurally diverse connections. Receptor-binding assays indicated satisfactory-to-excellentαVβ3 binding capabilities for most conjugates, while in vitro growth inhibition assays on a panel of human tumor cell lines revealed outstanding cell sensitivity values. Among the nine conjugate ensemble, derivative 21, bearing a robust triazole ring connected to ethylene glycol units by an amide function and showing excellent cell sensitivity properties, was selected for in vivo studies in an ovarian carcinoma model xenografted inimmunodeficient mice. Remarkable antitumor activity was attained, superior to that of PTX itself, which was associated with a marked induction of aberrant mitoses, consistent with the mechanism of action of spindle poisons. Overall, the novel cRGD-PTX conjugates disclosed here represent promising candidates for further advancement in the domain of targeted antitumor therapy.

***Br J Cancer*. 2012 Jul 10;107(2):360-9.**

Cisplatin plus paclitaxel and maintenance of bevacizumab on tumour progression, dissemination, and survival of ovarian carcinoma xenograft models.

Oliva P, Decio A, **Castiglioni V**, Bassi A, Pesenti E, Cesca M, Scanziani E, Belotti D, Giavazzi R.

BACKGROUND: Bevacizumab is being incorporated as first-line therapy with standard-of-care chemotherapy on epithelial ovariancarcinoma (EOC). We investigated bevacizumab combined with chemotherapy on tumour progression and mouse survival in EOC xenograft models.

METHODS: Bevacizumab was administered concomitantly with cisplatin plus paclitaxel (DDPþPTX), continued after induction(maintenance) or started after chemotherapy. The effect on tumour progression was monitored by bioluminescence imaging (BLI)(1A9-luc xenograft). Tumour dissemination into the peritoneal organs and ascites formation (HOC22 xenograft) was evaluated byhistological analysis at the end of treatment (interim) and at euthanasia (survival). The effects on overall survival (OS) were nvestigated in both EOC models.

RESULTS: Bevacizumab with PTXþDDP delayed tumour progression in mice bearing EOC xenografts. OS was significantly extended, with complete responses, by bevacizumab continued after stopping chemotherapy in the HOC22 xenograft. Bevacizumab alone inhibited ascites formation, with only limited effect on tumour burden, but combined with PTXþDDP reduced ascites and metastases. Bevacizumab started after induction with PTXþDDP and maintained was equally effective on tumour progression and survival on 1A9-luc xenograft.

CONCLUSION: Bevacizumab combined with chemotherapy not only affected tumour progression, but when administered as maintenance regimen significantly prolonged survival, reducing ascites, and tumour dissemination. We believe our findings are consistent with the clinical results and shed light on the potential effects of this kind of treatment on tumour progression.

***J Clin Endocrinol Metab*. 2013. [in press].**

Synergistic cooperation between sunitinib and cisplatin promotes apoptotic cell death in human medullary thyroid cancer.
Lopergolo A, Nicolini V, Cominetti D, Folini M, Perego P, **Castiglioni V**, Scanziani S, BorrelloMG, Zaffaroni N, Cassinelli G, Lanzi C.

PURPOSE: Tyrosine kinase (TK) inhibitors represent a new option for patients with advanced medullary thyroid cancer (MTC). However, cures have not been achieved with current available agents used in monotherapy. Since cisplatin can activate CD95 death receptor, we investigated the potential of the TK inhibitor sunitinib in combination with cisplatin to enhance apoptosis activation through the extrinsic pathway in Ret TK-dependent MTC preclinical models by exploiting the interplay of Ret with CD95-mediated pathway.
EXPERIMENTAL DESIGN: The effects of sunitinib and cisplatin, alone and in combination, were examined in human MTC cell lines harboring oncogenic RET mutations. In vitro and in vivo experiments were designed to explore drug activity on Ret signaling, cell growth, apoptosis, autophagy, tumor growth, and to investigate the mechanisms of the drug interaction.
RESULTS: Sunitinib and cisplatin synergistically inhibited the growth of MZ-CRC-1 cells harboring the RET M918T activating mutation. The two drugs in combination enhanced caspase activation through CD95-mediated apoptosis pathway. Sunitinib induced a perturbation of the autophagic flux characterized by autophagosome accumulation and a remarkable lysosomal dysfunction which was further enhanced, with likely leakage, by cisplatin. Administration of the two drugs in combination improved the antitumor efficacy against MZ-CRC-1 xenografts and increased apoptosis in tumor cells as compared to single agent treatments.
CONCLUSION: Preclinical evidence of a synergistic drug cooperation suggests that addition of cisplatin to sunitinib may be promising in a clinical combination treatment regimen for advanced sporadic or hereditary MTCs harboring the RET M918T oncogene.

ESVP/ECVP Meeting, London (UK), September 4th-7th 2013, poster presentation.

Immunohistological identification of disseminated tumor cells in the lungs of a mouse orthotopic xenograft model of human rhabdomyosarcoma.

Castiglioni V, De Maglie M, Rodighiero S, Cassinelli G, Lanzi C, Scanziani E, Recordati C.

INTRODUCTION: Murine xenografts are extensively used in the study of human malignancies. One of the major criticism of this animal model is its low metastatic potential. The aims of this study were to investigate a promising metastatic sarcoma model and to validate an immunohistological method able to detect human disseminated tumor cells in murine lungs.

MATERIALS AND METHODS: 7 SCID mice were injected intramuscularly with human A204 rhabdomyosarcoma cells and euthanized after 9 weeks. Standard histology, immunohistochemistry and immunofluorescence using specific anti-human Vimentin and MHCI antibodies were used for the assessment of tumor cell dissemination to the lungs.

RESULTS: Histological examination alone was not successful in identifying neoplastic dissemination to the lungs. Immunohistochemical methods enhanced the sensitivity of the analysis and both Vimentin and MHCI allowed to appreciate either single or clustered cells of human origin within pulmonary interstitium. Both markers co-localized in the same atypical cells with double-immunofluorescence.

CONCLUSION: Intramuscolar injection of A204 rhabdomyosarcoma cells can be regarded as a valuable metastatic orthotopic xenograft model. Double immunofluorescence using specific anti-human Vimentin and MHC I is a promising tool in the detection of pulmonary disseminated tumor cells.

Appendix 2: List of the scientific publications that do not involve human tumor xenografts.

***J Toxicol Pathol* [in press]**

Immunohistochemical characterization of a renal nephroblastoma in a Trp53-mutant and prolyl isomerase 1-deficient mouse.
Castiglioni V, De Maglie M, Queliti R, Rustighi A, Del Sal G, and Radaelli E.

A nephroblastoma is a tumor arising from metanephric blastema occurring in childhood. Among laboratory rodents, nephroblastoma has been frequently reported in rats, but it remains exceedingly rare in mice. The present work describes a nephroblastoma in a young mouse homozygous for the specific Trp53 R172H point mutation coupled with targeted deletion of the Pin1 gene. The affected kidney was effaced by a biphasic tumor with an epithelial component arranged in tubules surrounded by nests of blastemal cells. Immunohistochemically, the neoplasm was diffusely positive for Wilms' tumor antigen. The epithelial component expressed markers ofrenal tubular differentiation including wide-spectrum cytokeratin, E-cadherin and folate-binding protein. Furthermore, the neoplasm exhibited a high proliferative index and diffuse nucleocytoplasmic β-catenin expression. Based on histological and immunohistochemical features, a diagnosis of nephroblastoma potentially associated with Trp53 loss and oncogenic β-catenin activation has been proposed.

Vet Microbiol. **2012 Sep 14;159(1-2):107-14.**

Enterohepatic Helicobacter spp. in colonic biopsies of dogs: molecular, histopathological and immunohistochemical investigations.

Castiglioni V, Vailati Facchini R, Mattiello S, Luini M, Gualdi V, Scanziani E, Recordati C.

Enterohepatic Helicobacter spp. have been described colonizing the large intestine and liver of healthy and symptomatic subjects and are thought to have a role in the development of inflammatory bowel disease (IBD). The prevalence of enterohepatic Helicobacter spp. infection in dogs is largely unknown and to our knowledge there are no data about their potential pathogenic role. In light of these considerations, the aims of this study were (i) to assess the prevalence of enterohepatic Helicobacter spp. in colonic biopsies of symptomatic pet dogs and (ii) to evaluate a possible association between Helicobacter spp. colonization status (heavily colonized, poorly colonized and uncolonized biopsies) and histological lesions. Colonic biopsies from 27 pet dogs of different ages were evaluated by family Helicobacteraceae and enterohepatic Helicobacter spp. PCR, histology,and immunohistochemistry for the in situ detection of Helicobacter spp. organisms. 85%and 52% of colonic biopsies were positive by Helicobacteraceae and enterohepatic Helicobacter spp. PCR, respectively. Immunohistochemistry revealed Helicobacter spp. were localized both in the superficial mucus (55%) and within intestinal crypts (33%). Dogs with heavy enterohepatic Helicobacter spp. colonization were significantly younger and had a higher level of mucosal fibrosis/atrophy than dogs with uncolonized or poorly colonized biopsies ($p < 0.05$). These findings contribute to widen current knowledge regarding canine enterohepatic Helicobacter spp., suggesting the infection is rather common in dogs and acquired at an early age. Furthermore, heavy colonization of colonic crypts is associated with chronic inflammatory lesions (fibrosis/atrophy), supporting the role of enterohepatic Helicobacter spp. in the development of canine IBD.

***Vet Rec*. 2012 Mar 24;170(12):312.**

Long-term study of MRSA ST1, t127 mastitis in a dairy cow.
Pilla R, **Castiglioni V**, Gelain ME, Scanziani E, Lorenzi V, Anjum M, Piccinini R.

METICILLIN-resistant Staphylococcus aureus (MRSA) has been reported in human medicine as a cause of nosocomial and community-associated infections (Otter and French 2010). In veterinary medicine, MRSA strains have been identified in a wide range of animals and diseases(Leonard and Markey 2008, Fessler and others 2009, Huber and others2010, Turkyilmaz and others 2010), thus it is considered an emerging threat with a high zoonotic potential (Juhasz-Kaszanyitzky and others2007). MRSA sequence type (ST) 1, spa type (t) 127 has been mostly isolated from community-associated infections, but t127 has seldom been identified in cattle and pigs (Hasman and others 2010).The present report regards a dairy cow with an intramammary infection by MRSA ST1, t127 that was investigated over an entire lactation and submitted to histological evaluation of mammary tissue to explore both bacterial molecular features and host immune response in the milk and mammary tissue. The study was performed because only a few mammary infections of the dairy cow by this particular strain have been reported and no information is available on the interaction between the bacteria and the mammary gland.

***Res Vet Sci*. 2011 Oct;91(2):251-3.**

Outbreak of bovine clinical mastitis caused by Mycoplasma bovis in a North Italian herd.

Radaelli E, **Castiglioni V**, Losa M, Benedetti V, Piccinini R, Nicholas RA, Scanziani E, Luini M.

This report describes an outbreak of Mycoplasma bovis mastitis affecting 45 cows in a herd of 122 dairy cattle in Northern Italy. Clinically, the outbreak was characterized by agalactia, multiple swollen and painless quarters, high milk somatic cell count and unresponsiveness to conventional antibiotic therapy.M. bovis was isolated from the milk samples of all the 32 affected cows tested and from the mammary tissue of three affected cows that underwent necropsy. No other pathogens were isolated from these samples. Lesions in two of the necropsied cows were characterized by mild chronic suppurative mastitis and galactophoritis. The other necropsied cow showed a chronic necrosuppurative and pyogranulamaous galactophoritis, a condition not previously associated with M. bovis. M. bovis was detected immunohistochemically in the lumen of the affected mammary ducts suggesting that ascending infection via the teat canal was the likely route of transmission. No other intralesional pathogens were demonstrated microscopically.

***Histol Histopathol*. 2011 Mar;26(3):285-96.**

Clinical, pathological and immunological features of psoriatic-like lesions affecting keratin 14-vascular endothelial growth factor transgenic mice.

Canavese M, Altruda F, Silengo L, **Castiglioni V**, Scanziani E, Radaelli E.

Up-regulation of vascular endothelial growth factor (VEGF) plays a primary role in the pathogenesis of psoriasis. Transgenic mice over-expressing VEGF under the Keratin 14 (K14) promoter develop an inflammatory skin condition with many of the pathobiological features of human psoriasis. In this work, the development of spontaneous psoriatic-like dermatitis in K14-VEGF transgenic mice was monitored from week 6 to week 44 and skin lesions were characterized clinically (application of a clinical score system comparable to the human Psoriasis Area and Severity Index), microscopically (histopathology, leukocyte subset and neoangiogensis) and immunologically (evaluation of local and systemiccytokine/chemokine profiles).Based on PASI score system, three progressive clinical phases were identified: mild acute (8-14 weeks of age), moderate subacute (15-21 weeks of age) and severe chronic-active (22-44 weeks of age) dermatitis. Microscopically, skin lesions consisted of progressive proliferative psoriatic-like dermatitis dominated by dermo-epidermal infiltrates of CD3-positivelymphocytes, an increased number of mast cells and neoangiogenesis. Both local and systemic up-regulation of pro-inflammatory (IL-12, TNF-alpha, IL-6, MCP-1and IL-8) and regulatory (IL-10) cytokines/chemokines was observed, mainly during the later stages of disease development. The results obtained in this study further confirm the central role of VEGF over-expression in the development of psoriatic-like dermatitis. Similarly to what is reported for human psoriasis, both the local and systemic immunologic profiles observed in K14-VEGFtransgenic mice suggest that a combined Th1 and Th17response may be implicated in lesion development. The identification of three progressive stages of disease, each with peculiar clinicopathological features, renders theK14-VEGF transgenic mouse a valuable model to study novel immunotherapies for psoriasis.